Effect, number and location of synapses made by single pyramidal cells onto aspiny interneurones of cat visual cortex

E. H. Buhl*, G. Tamás*†, T. Szilágyi*‡, C. Stricker§, O. Paulsen* and P. Somogyi*

*MRC Anatomical Neuropharmacology Unit, Department of Pharmacology, University of Oxford, Mansfield Road, Oxford OX1 3TH, UK, †Department of Zoology and Cell Biology, József Attila University, Szeged, Hungary, ‡Department of Physiology, University of Medicine and Pharmacy, Târgu Mures, Romania and §Division of Neuroscience, The John Curtin School of Medical Research, Australian National University, Canberra, ACT 0200, Australia

1. Dual intracellular recordings were made from synaptically coupled pyramidal cell-to-interneurone pairs ($n = 5$) of the cat visual cortex *in vitro*. Pre- and postsynaptic neurones were labelled with biocytin, followed by correlated light and electron microscopic analysis to determine all sites of synaptic interaction.

2. Pyramidal neurones in layers II–III elicited monosynaptic EPSPs in three distinct classes of smooth dendritic local-circuit neurones, namely basket cells ($n = 3$), a dendrite-targeting cell ($n = 1$) and a double bouquet cell ($n = 1$). Unitary EPSPs in basket cells were mediated by one, two, and two synaptic junctions, whereas the pyramid-to-dendrite-targeting cell and pyramid-to-double bouquet cell interaction were mediated by five and seven synaptic junctions, respectively. Recurrent synaptic junctions were found on all somato-dendritic compartments, with a tendency to be clustered close to the soma on the double bouquet and dendrite-targeting cells. The latter interneurones were reciprocally connected with pyramidal cells.

3. Unitary EPSPs had an average peak amplitude of 1005 ± 518 μV, fast rise times (10–90%; $0{\cdot}67 \pm 0{\cdot}25$ ms) and were of short duration (at half-amplitude, $4{\cdot}7 \pm 1{\cdot}0$ ms). Their decay was monoexponential ($\tau = 7{\cdot}8 \pm 4{\cdot}3$ ms) at hyperpolarized membrane potentials and appeared to be shaped by passive membrane properties ($\tau = 9{\cdot}2 \pm 8{\cdot}5$ ms). All parameters of concomitantly recorded spontaneous EPSPs were remarkably similar (mean amplitude, 981 ± 433 μV; mean rise time, $0{\cdot}68 \pm 0{\cdot}18$ ms; mean duration, $4{\cdot}7 \pm 1{\cdot}7$ ms).

4. In all three pyramidal-to-basket cell pairs, closely timed (10–50 ms) pairs of presynaptic action potentials resulted in statistically significant paired-pulse depression, the mean of the averaged second EPSPs being 80 ± 11% of the averaged conditioning event. The overall degree of paired-pulse modulation was relatively little affected by either the amplitude of the preceding event or the inter-event interval.

5. The probability density function of the peak amplitudes of the unitary EPSPs could be adequately fitted with a quantal model. Without quantal variance, however, the minimum number of components in the model, excluding the failures, exceeded the number of electron microscopically determined synaptic junctions for all five connections. In contrast, incorporating quantal variance gave a minimum number of components which was compatible with the number of synaptic junctions, and which fitted the data equally well as models incorporating additional components but no quantal variance. For this model with quantal variance with the minimum number of components the estimate of the quantal coefficient of variation ranged between 0·33 and 0·46, and the corresponding quantal sizes ranged between 260 and 657 μV. The peak EPSP amplitudes in two of the four connections with more than one synaptic junction could be adequately described by a uniform binomial model for transmitter release.

6. In conclusion, at least three distinct interneurone classes receive local excitatory pyramidal cell input which they relay to different compartments on their postsynaptic target neurones. The reliability of transmission is high, but the fast time course of the EPSPs constrains their temporal summation. Due to the relatively small amplitude of unitary EPSPs several convergent inputs will therefore be required to elicit suprathreshold responses.

There is ample evidence that in cortical areas GABAergic local-circuit neurones provide the major source of intrinsic inhibition (for review see Somogyi, 1989). Overall these neurones play a vital role in modulating glutamate-mediated excitation, although this relatively global concept is inadequate to explain the anatomical and neurochemical heterogeneity of *GABAergic aspiny local-circuit neurones* (for reasons of brevity subsequently referred to as *'interneurones'*), as reflected in the diversity of their connections. Thus, circumscript classes of interneurones may subserve distinct functional roles. For example, the association of GABAergic axons with subsets of excitatory afferents strongly suggests a pathway-specific modulatory function (Han, Buhl, Lörinczi & Somogyi, 1993). Other interneurones that preferentially innervate the perisomatic domain of principal cells appear to have an important role in synchronizing sub- and suprathreshold population activity, as demonstrated in the hippocampus (Cobb, Buhl, Halasy, Paulsen & Somogyi, 1995). Not surprisingly, this apparent division of labour is paralleled by differences in the excitatory inputs and activation of GABAergic neurones. Due to the geometry of their dendrites certain types of interneurones in the hippocampal molecular layer may only be activated in a feedforward manner (Han *et al.* 1993). Others, such as the somatostatin- and metabotropic glutamate receptor (mGluR1α)-positive interneurones, receive predominantly, if not exclusively, recurrent excitatory input (Maccaferri & McBain, 1995), whereas some cell classes, such as basket neurones, are presumably involved in both types of circuit (Buhl, Halasy & Somogyi, 1994).

These recent advances indicate salient principles governing the flow of information involving GABAergic cortical micro-circuits. Evidently, much of this progress has emerged from work undertaken in the hippocampal cortex and novel insights have been facilitated by the laminar arrangement of its excitatory afferents and the geometric alignment of its principal neurones. It has been considerably more difficult to establish whether similar rules apply for neocortical areas, where a more complex cyto-architecture provides a greater challenge for conceptual progress. Nevertheless, it was in cat visual cortex that it was established that the efferent output of GABAergic cell types is targeted to specific domains on their postsynaptic neurones (Somogyi, 1989). Subsequent work, largely done in the rat neocortex, has demonstrated that some interneurones show distinct physiological properties which are paralleled not only by their morphology but also by their neurochemical identity (Kawaguchi & Kubota, 1993). Moreover, several recent studies have focused on synaptic communication between physiologically and anatomically identified rat neocortical neurones (Deuchars & Thomson, 1995; Thomson, West & Deuchars, 1995). Some of this work, for example, has provided evidence that in the rat somatosensory cortex unitary connections between pyramidal neurones differ from pyramid-to-interneurone interactions with respect to the degree of paired-pulse modulation (Thomson, Deuchars & West, 1993*a*, *b*).

When addressing experimental questions regarding the functional properties of identified GABAergic neurones, cat visual cortex appears to be suitable for two major reasons. First, detailed work has been done to investigate GABAergic local-circuit neurones (for review see Somogyi, 1989), whereas in the rat visual cortex the equivalent cell types remain considerably less well defined. Second, three decades of intense research have elucidated many of the physiological properties of cat visual cortex. Several of these studies have already highlighted the importance of GABAergic circuits in shaping the functional characteristics of cortical neurones (Eysel, Crook & Machemer, 1989; for review see Sillito, 1992) and numerous specific models and wiring diagrams have been put forward (e.g. Erwin, Obermayer & Schulten, 1995), although the majority of them remain to be tested experimentally.

In this study, using an *in vitro* preparation of cat visual cortex, we have focused on the local recurrent excitatory input to identified interneurones within layers II–IV, addressing the following questions. Which types of interneurones receive local excitatory feedback? Is the recurrent input targeted to a particular domain of the postsynaptic somato-dendritic surface? What are the properties of recurrent unitary EPSPs? What is the strength of individual connections? Which factors contribute to the variability of postsynaptic responses? These issues were investigated by employing paired intracellular recordings, followed by correlated light and electron microscopy and eventually attempting to synthesize the available anatomical and physiological information, thus aiming towards a functional interpretation of synaptic communication. Some of the results have been presented in abstract form (Buhl, Tamás & Somogyi, 1995; Buhl, Tamás, Szilágyi, Paulsen & Somogyi, 1996; Paulsen, Stricker, Tamás, Szilágyi, Somogyi & Buhl, 1996). Those results which detail interneurone-to-pyramidal cell connections are reported in the accompanying paper (Tamás, Buhl & Somogyi, 1997).

METHODS

Slice preparation

Adult female cats weighing 2·6–3·2 kg were deeply anaesthetized with an intramuscular injection of ketamine (30 mg kg^{-1}) and xylazine (10 mg kg^{-1}). Following the cessation of pain reflexes, such as the pedal withdrawal reflex and/or noxious tail pinch, a bilateral craniotomy was performed to expose the occipital poles of the cerebral hemispheres, but leaving the dura intact. After once more ensuring adequate levels of anaesthesia by ascertaining the loss of noxious pain reflexes (see above) the animals were immediately killed by intracardial perfusion with approximately 1·5 l of chilled and oxygenated artificial cerebrospinal fluid (ACSF) which was initially composed of (mM): 252 sucrose, 3·0 KCl, 1·25 NH_2PO_4, 24 $NaHCO_3$, 2·0 $MgSO_4$, 2·0 $CaCl_2$ and 10 glucose (Buhl *et al.* 1994). Then the dura was opened and blocks of brain tissue, containing areas 17 and 18, were carefully removed and immersed in chilled ACSF. Using a vibroslice (Campden Instruments, Loughborough, UK) 400 μm thick slices were cut at an orientation approximately perpendicular to the medial and dorsal surfaces of the occipital pole. Thus the majority of radially oriented

interlaminar circuits appeared to be optimally preserved. The resulting slices were transferred to a recording chamber where they were maintained at 34–35 °C on a nylon mesh at the interface between oxygenated ACSF and a humidified atmosphere saturated with 95% O_2–5% CO_2. Following 30–45 min of recovery in modified ACSF, the latter was eventually changed to normal ACSF by replacing all sucrose with equiosmolar NaCl (126 mM), leaving other electrolytes unchanged.

Intracellular recording and data analysis

Recording electrodes were pulled from standard wall borosilicate tubing (1·2 mm o.d., 0·69 mm i.d., with inner filament; Clark Electromedical Instruments, Pangbourne, UK) using a Flaming Brown-type horizontal puller (model P-87, Sutter Instruments, Novato, CA, USA) and filled with 1·5 M KCH_3SO_4 containing 2% biocytin (Buhl *et al.* 1994). These micropipettes were generally bevelled at an angle of 27 deg from the vertical to a DC resistance of 60–150 MΩ (BV-10 Microelectrode Beveller, Sutter Instruments). Recordings were obtained from layers II–IV within areas 17 and 18 of the visual cortex. Initially a search was made, by using a mechanical micromanipulator in a vertical axis, for putative interneurones displaying characteristic properties, such as short-duration action potentials, large-amplitude after-hyperpolarizing potentials and modest or missing spike frequency adaptation. Those cells which required a continued hyperpolarizing bias current to prevent spontaneous generation of action potentials were abandoned. Once a stable recording had been obtained, a second microelectrode was advanced into the tissue with a motorized stepper at an angle of 30–40 deg from the vertical, usually in relatively close proximity (< 400 μm) to the first electrode track. Following the impalement of a sufficiently stable neurone with the physiological characteristics of a cortical principal cell (e.g. broader action potentials, depolarizing and/or late hyperpolarizing after-potentials, and spike frequency adaptation) the cells were tested for synaptic coupling by eliciting single action potentials with rheobasic depolarizing current pulses (in the range 0·1–0·5 nA) in one of the neurones, whilst monitoring the membrane response in the second neurone, using on-line spike triggered averaging ($n \geqslant 32$). No attempt was made to either quantify or characterize further those dual impalements in which no measurable (< 100 μV) synaptic response was detectable. The occurrence of synaptic coupling was generally tested both ways and synaptic responses evoked in the pyramidal cell by action potentials in the interneurone are detailed in the accompanying paper (Tamás *et al.* 1997). Moreover, the companion paper also contains a description of all anatomical procedures.

Capacitive electrode coupling artefacts were eliminated on-line using a modified (Mason, Nicoll & Stratford, 1991) Axoprobe amplifier (Axon Instruments). Once synaptic coupling had been established, single action potentials or bursts of action potentials were elicited with depolarizing current pulses at frequencies ranging from 1 to 3 Hz. Whenever pairs of presynaptic action potentials were evoked, usually at 1 Hz, these were separated by intervals of 10–60 ms duration. The experimental data were acquired using a PCM-701ES instrumentation recorder (Intracel, Shepreth, UK) and stored on videotapes. Subsequently, the recordings were redigitized off-line at 10–20 kHz using 12 bit A/D boards (RC Electronics Computerscope, Santa Barbara, CA, USA and National Instruments Labmaster+, Newbury, UK). All data used to determine kinetic properties, average amplitudes and paired-pulse measurements were low-pass filtered at 1 kHz, whereas those data used for quantal analysis were filtered at frequencies between 0·2 and 1 kHz, after empirically determining which filtering parameters resulted in the best signal-to-noise ratio. Although harsher filtering clearly slowed the measured EPSP rise times, the respective peak amplitudes remained largely unaffected (reduction < 5%). Subsequent data analysis was performed with Axograph (Axon Instruments), RC Electronics Computerscope (RC Electronics), WCP (courtesy of Dr J. Dempster, University of Strathclyde, UK) and Igor Pro (WaveMetrics, Lake Oswego, OR, USA) software packages. Values are generally expressed as means ± S.D.

Resting membrane potentials were determined following electrode withdrawal and are given as the difference between surface DC potential and the steady-state membrane potential without bias current. Membrane time constants were obtained by fitting a single exponential to the decay of brief (< 20 ms), small-amplitude hyperpolarizing current pulses (−0·1 nA). Input resistances were determined from measuring the maximal voltage deflection of 200 ms duration averaged −0·1 nA hyperpolarizing current pulses. When excluding a brief period (~2 ms) following the peak of unitary and spontaneous EPSPs, their decay phase could be adequately (judged by eye) fitted with single exponentials. For paired-pulse amplitude measurements, all synaptic events were aligned on the rising phase of the first presynaptic action potential and subsequently, due to variations of the interspike intervals, re-aligned on the rising phase of the successive second action potential. Then the respective voltage traces of the postsynaptic cell were averaged over each of four equal-length periods, with those used for noise and EPSP measurements separated by equal intervals. Average voltages for the first two periods preceding the synaptic event were calculated for each sweep and their respective differences provided the noise sample distribution. Likewise, EPSP peak amplitude measurements were obtained from the set of differences between the average voltage of a period preceding the EPSP and the time window encompassing the peak of the EPSP. Due to the relatively brief interspike intervals (< 70 ms) which were employed to evoke paired-pulse modulation of unitary EPSPs, the on-going decay of the first, conditioning EPSPs could significantly overlap with the rise of the successive event, essentially arising from a sloping baseline and therefore affecting the measurements of the second EPSP. Assuming linear summation of the recorded voltage, the amplitude measurements which were obtained for the second EPSP (all events ⩾ 2 S.D. values of noise) were corrected for the extrapolated decay of the preceding EPSP, taking into account the respective interspike interval as well as the peak amplitude and monoexponential decay kinetics of the conditioning event.

Analysis of amplitude fluctuations of EPSPs

Peak amplitude measurements for quantal analysis of the EPSPs were made by calculating the difference between two single point measurements of each digitized trace. The time points were selected by placing two cursors on the average trace for the epoch under study visualized on a computer display. One cursor was placed on the baseline with a fixed latency. The exact position of this cursor depended on the degree of baseline distortion due to the coupling artefact and could be in a location either preceding or following the presynaptic action potential. Likewise, the second cursor was set at a position corresponding to the peak of the averaged EPSP (Fig. 8*Aa–c*). Corresponding noise measurements were made between pairs of points during the baseline period before each event using the same separation in time between the measuring points. In order to improve the noise estimate, for some pairs of cells up to four noise measurements were obtained from each pre-event baseline. Data were used only from epochs of recording when the postsynaptic responses remained stationary, defined as epochs during which the mean amplitude of sixty

consecutive EPSPs remained within ± 1 S.D. of the mean amplitude of the first sixty EPSPs within the epoch (Fig. 8*Ba*).

Quantal analysis by noise deconvolution was made following the procedure of Stricker, Redman & Daley (1994). First, the noise was estimated as the sum of two Gaussian functions fitted by a maximum likelihood criterion (Fig. 8*Ca*; Stricker *et al.* 1994). Second, the probability density function of the EPSP and noise amplitudes were represented as a Gaussian kernel density estimate, where the variance of the kernel was dependent on the baseline noise and the anticipated quantal amplitude, as described in Stricker *et al.* (1994). For purposes of presentation only, the EPSP amplitudes are shown as amplitude frequency histograms scaled as a probability density (Figs 8*C* and 9). Third, three different models for amplitude fluctuations were fitted to the EPSP densities by a maximum-likelihood criterion using the expectation–maximization (E–M) algorithm (Stricker *et al.* 1994). These models were: a sum of double Gaussian functions with variances equal to those of the noise (fully unconstrained noise deconvolution; Fig. 8*Cb*), a sum of double Gaussian functions with means separated by a constant increment and variances equal to those of the noise (quantal model without quantal variance; Fig. 8*Cc*), and a sum of components with means separated by a constant increment and variances equal to the sum of the noise variances and an additional quantal variance term (quantal model with type I quantal variance; Walmsley, 1993; Fig. 8*Cd*). No constraints were made for the amplitude probability of any component at this stage.

The different models were compared by use of the log-likelihood ratio as a test statistic (Wilks statistic; Wilks, 1938). The significance level for rejection was obtained by comparing the actual log-likelihood ratio with a log-likelihood ratio distribution. When the models were nested, i.e. when one model could be transformed to the other by a smooth parametric transition, the log-likelihood ratio distribution approaches the χ^2 distribution and this χ^2 distribution with the appropriate degrees of freedom was used accordingly to evaluate the significance level (P). When the models were not nested, the log-likelihood ratio distribution was estimated by fitting the two competing models to each of 250 Monte Carlo samples from the model serving as null hypothesis as described in Stricker *et al.* (1994). The decision as to which model was appropriate was based on the assumption that the simplest (i.e. the model with the least number of parameters), but still statistically adequate description of the data (parsimony), identifies the best model. For this model, balanced resampling techniques were used to obtain confidence limits for model parameters (Davison, Hinkley & Schechtman, 1986). The original data set was resampled randomly, with replacement, to obtain 100 samples, each with the same size as the original sample. The E–M algorithm was applied to the probablility density function formed by each resampling, and the parameter set obtained in this way was used to estimate the S.D. of each parameter.

For the fully unconstrained model, the smallest number of components which was necessary to fit the amplitude distribution was determined by repeating the maximum likelihood estimation for increasing numbers of components. The smallest number of components was defined as the number to which the addition of a further component did not significantly improve the fit ($P > 0{\cdot}05$; Wilks statistic). Each of the two quantal models was then tested against the fully unconstrained deconvolution. In this test, the quantal models were made null hypotheses, and the fully unconstrained model was the alternative. For the quantal model without quantal variance, the number of double Gaussian functions was the same as for the fully unconstrained model. For the quantal model with quantal variance, the smallest number of components was determined, for which an increment of one component did not significantly improve the fit, and for which the fully unconstrained model was not significantly better ($P > 0{\cdot}05$; Wilks statistic).

RESULTS

Although it was generally feasible to tentatively identify cortical interneurones by virtue of their physiological properties, such as short-duration action potentials (< 0·5 ms at half-amplitude), this strategy occasionally resulted in the labelling of excitatory principal neurones. Therefore, following histological analysis only those unitary excitatory interactions were preselected in which the communicating cells could be unambiguously attributed to a spiny presynaptic neurone and a postsynaptic smooth-dendritic neurone ($n = 10$). Subsequently, however, only those interactions will be described in which we obtained long-duration stable recordings as well as the electron microscopic correlate for the number of synaptic release sites ($n = 5$). One additional connection is briefly presented in which it was not possible to electron microscopically identify the sites of synaptic interaction. Apart from a pyramidal neurone with incomplete filling of its dendritic arbor, the remainder of cells, within the confines of the slice, appeared to be completely labelled, without appreciable tapering of the reaction product towards the distal tips of dendrites and axons. Further light microscopic scrutiny indicated that the relatively small dimensions and compactness of interneuronal

Figure 1. Pyramid-to-dendrite-targeting cell pair 1612941

A, reconstruction of a synaptically coupled layer III–IV border pyramid (black) and a layer IV dendrite-targeting cell (red). *B*, for clarity of display the pyramidal cell axon and interneurone dendrites have been shifted to the right. *C*, after omitting all non-contacting side branches (asterisks) it becomes apparent that all synaptic junctions were provided by 2 ascending pyramidal cell axon collaterals. *D*, the latter established a total of 5 synaptic junctions on 4 segments of three dendrites, all in close proximity to the interneurone cell body. The dendrite-targeting cell was reciprocally connected with the pyramidal cell (see Tamás *et al.* 1997). *Ea*, averaged pyramidal cell action potential (for clarity of display a part of the trace containing the smeared capacitance artefact has been replaced by a dashed line). *Eb*, pyramidal cell activity elicited a short-latency EPSP in the postsynaptic neurone. *Ec*, successive superimposed EPSPs show considerable fluctuation in their amplitudes. *Ed*, the late phase of the averaged EPSP was characterized by a mono-exponential decay back to baseline. *Ee*, average of spontaneous EPSPs, also showing a monoexponential decay.

Figure 1. For legend see facing page.

Table 1. Postsynaptic target distribution of five identified neocortical interneurones

Cell pair	Postsynaptic interneurone	Interneurone postsynaptic targets (%) Soma	Dendritic shaft	Dendritic spine	Number of tested synapses*
0812945	BC	46·2	53·8	0·0	13
1102941	BC(4)†	35·3	58·8	5·9	17
0812942	BC(3)	61·5	34·6	3·8	26
1612941	DTC(1)	4·2	83·3	12·5	24
1412942	DBC(1)	0·0	36·0	64·0	25

*Random samples of electron microscopically identified postsynaptic elements; †serial numbers in accompanying paper (Tamás *et al.* 1997). BC, basket cell; DTC, dendrite-targeting cell; DBC, double bouquet cell.

dendritic trees favoured their virtually complete recovery. Likewise, numerical estimates (see Tamás *et al.* 1997) indicate that the axonal clouds, of at least those interneurones contained within our sample, were representative of the class of local-circuit neurone (for detail see Tamás *et al.* 1997) and relatively unaffected by the slicing procedure. It is considerably more likely, however, that a substantially greater proportion of the relatively wide-ranging axonal arbor of layer III pyramidal cells (Gilbert, 1983) has been truncated during slice preparation. Therefore, we cannot exclude the possibility that in the intact brain some of the interneurones may have received a larger number of recurrent pyramidal cell synapses from axon collaterals, although this scenario is unlikely, considering the relatively straight, radiating trajectory of pyramidal cell axon collaterals (Kisvarday, Martin, Freund, Magloczky, Whitteridge & Somogyi, 1986).

In all instances, the respective pre- and postsynaptic neurones were graphically reconstructed in their entirety and every site of light microscopically detected membrane apposition between a pyramidal cell axon and the dendrites of the postsynaptic local-circuit neurone was scrutinized in serial electron microscopic sections. The anatomical identification of synaptic contacts, their numbers as well as their placement, should therefore represent an accurate structural correlate of the unitary EPSPs. Due to the relevance of these parameters for the interpretation of the physiological data, the anatomical analysis of the connections is presented first.

Patterns of recurrent pyramid-to-interneurone connections

All presynaptic spiny or principal cells were located in layers II–III, including two layer III–IV border pyramids. The efferent synaptic target profile of the respective interneurones was determined by random electron microscopic sampling of elements, such as dendrites or spines, which were postsynaptic to the interneurone axon (Table 1; for further technical details see Tamás *et al.* 1997). These data clearly indicate that the cells fall into three distinct anatomical categories. The respective members of these

Figure 2. Light and electron microscopic evidence for five synaptic junctions mediating a unitary recurrent EPSP (cell pair 1612941 – see Fig. 1)

A, light micrograph showing boutons 1, 2 and 5 (numbering corresponding to Fig. 1*D*) in close apposition to an interneurone dendrite (d). *Aa*, low power electron micrograph showing two of the pyramidal cell boutons (b1 and b2) in synaptic contact with the interneurone dendrite (d). Both pre- and postsynaptic elements can be readily recognized due to their content of an electron dense precipitate. *Ab–d*, high power electron micrographs showing 3 synaptic junctions established by boutons b1, b2 and b5, respectively. All presynaptic terminals contain synaptic vesicles. Note the presence of a perforation (p) in the synaptic junction established by bouton b2 (in *Ac*). White arrows demarcate the extent of synaptic membrane specializations. *B*, light micrograph showing bouton b3 juxtaposed to a varicose swelling of a proximal interneurone dendrite (d). *Ba*, electron micrograph showing the synaptic junction (delineated by white arrows) established by bouton b3. In the same ultrathin section two unlabelled terminals (t) can be seen to establish asymmetrical synaptic junctions (between white arrowheads) with a dendritic protrusion, which is also apparent in *B*. *C*, light microscopically visualized apposition of bouton b4 and the proximal portion of a dendritic shaft (d). *Ca*, corresponding electron micrograph showing the synaptic junction established by bouton b4 on the dendrite-targeting cell. Scale bars in *A–C*, 5 μm; *Aa*, 0·5 μm; *Ab*, 0·2 μm (also applies to *Ac*, *d* and *Ca*); *Ba*, 0·2 μm.

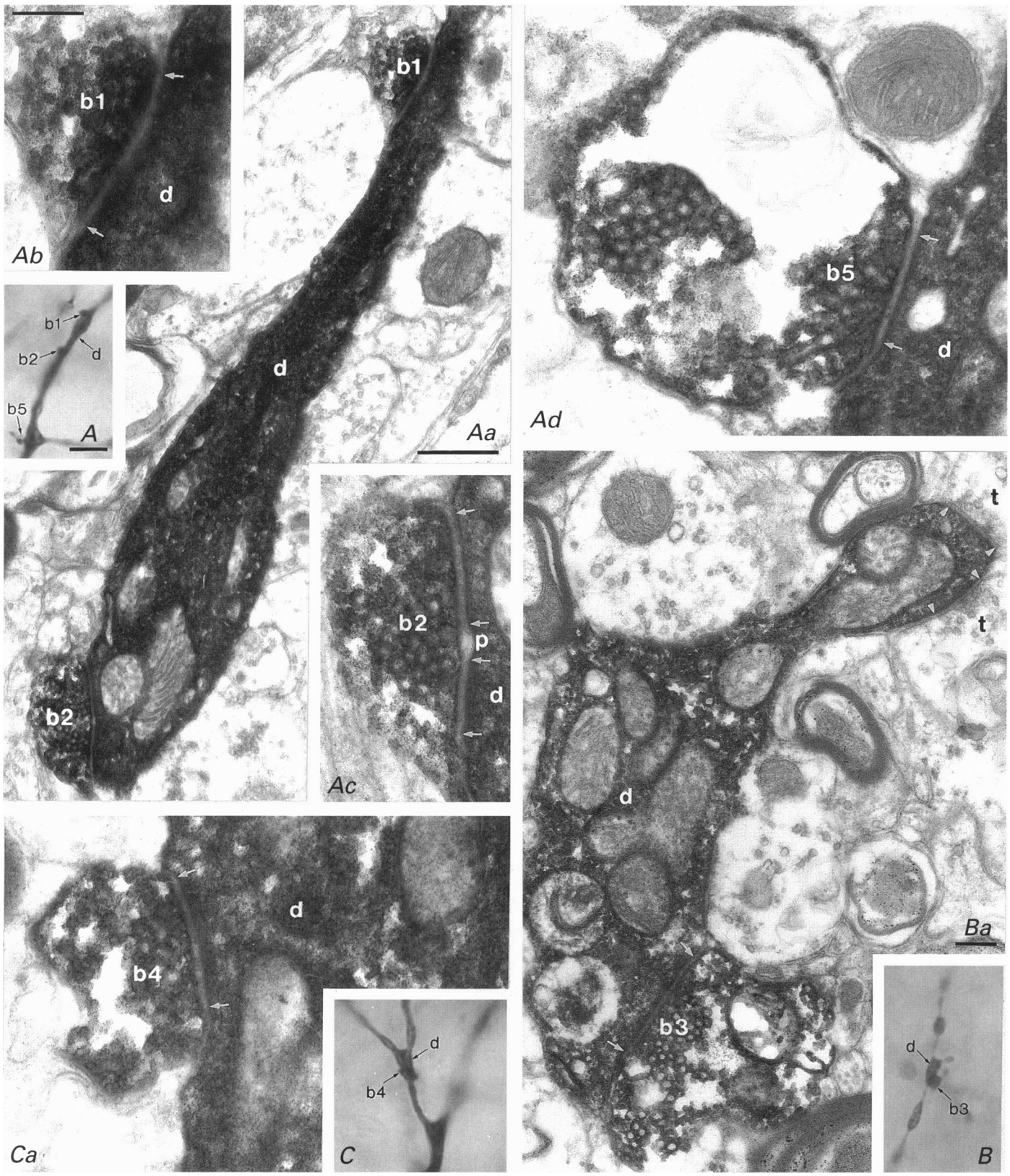

Figure 2. For legend see facing page.

classes were a layer IV dendrite-targeting cell (cell pair 1612941), three layer II–III basket cells (cell pairs 1102941, 0812942, 0812945), and a layer II–III double bouquet cell (cell pair 1412942). Two of the five pairs were found to be reciprocally connected with the presynaptic pyramids (1612941 and 1412942; for further details see Tamás *et al.* 1997).

Pyramid-to-dendrite-targeting cell pair 1612941. Although similar in its appearance to previously described layer IV clutch cells (Kisvarday, Martin, Whitteridge & Somogyi, 1985), the postsynaptic interneurone was identified as a layer IV dendrite-targeting cell (Fig. 1*A* and *B*), with electron microscopic sampling of postsynaptic targets indicating that 96% of the efferent output was directed towards dendrites or spines (Table 1). The dendrite-targeting cell had the majority of its smooth dendrites confined to layer IVa, although several branches invaded the lower portion of layer III (Fig. 1*B*). Similarly, much of the axonal arbor ramified within layer IVa, with a significant proportion entering lower layer III. One descending axonal branch traversed layer IVb and gave rise to a small cloud of terminal branches within layers V and VIa (Fig. 1*A*). The presynaptic pyramidal cell was positioned at the border of layers III–IV (Fig. 1*A*), having all basal dendritic branches contained within layer IVa, whereas most ascending dendrites ramified in lower layer III. The apical dendrite bifurcated and both daughter branches established a small dendritic tuft within layer I. The descending axon of the pyramidal cell gave rise to four collaterals, two of which ascended towards the dendrite-targeting cell (Fig. 1*C*) establishing a total of five synaptic junctions (two and three, respectively) with three ascending dendrites of the dendrite-targeting cell (Fig. 1*D*). One of the dendrites received one synapse (no. 5) on the primary trunk and two additional ones more distally on a daughter branch. Thus, in this cell, a total of four dendritic segments received the recurrent input. Despite the variability of pre- and postsynaptic elements it is, however, interesting to note that all synaptic sites were clustered in a very narrow, proximal region of the dendritic arbor of the dendrite-targeting cell.

Electron microscopic verification of synaptic junctions. For reasons of brevity, the presentation of electron microscopic evidence (Fig. 2) has been restricted to the interaction between the pyramidal neurone and the dendrite-targeting cell (1612941) described above. However, for this representative example the correlated light as well as electron microscopic evidence for *all* five synaptic release sites is illustrated. During the light microscopic analysis and ensuing graphical reconstruction of this pyramid-to-interneurone pair each possible contact site between pre- and postsynaptic neurone ($n = 7$) was carefully mapped, photographed (Fig. 2*A–C*; note that only those sites which were shown to establish a synaptic junction are illustrated) and subsequently re-embedded for electron microscopic analysis. Utmost care was taken to either verify electron microscopically the presence of single, but also multiple, synaptic junctions, or alternatively exclude those sites where the pre- and postsynaptic neurone formed no apparent synaptic junction. When scrutinizing ultrathin sections in the electron microscope, cross-sectioned profiles of pre- and postsynaptic elements were readily recognizable due to their cytoplasmic labelling with electron dense precipitate (e.g. Fig. 2*Ac*). Moreover, when juxtaposed, the overall correspondence between light and electron micrographs was apparent (e.g. Fig. 2*A vs. Aa*, *B vs. Ba*).

In this material, synaptic junctions between pyramidal cell axon terminals and postsynaptic interneurones were thus identified by adhering to the following criteria: (1) accumulation of synaptic vesicles in a presynaptic bouton; (2) rigid apposition of the pre- and postsynaptic membranes in conjunction with a widening of the extracellular space; and (3) the presence of a pre- and/or postsynaptic membrane specialization, when detectable. After tracing all possible contact sites through consecutive 70 nm serial ultrathin sections it was eventually possible, for all five cell pairs, to either verify or refute the corresponding light microscopic predictions. In all instances the number of light microscopically predicted sites of interaction exceeded the number of electron microscopically detected synaptic junctions by, on average, $63 \pm 37\%$. In contrast to

Figure 3. Pyramid-to-basket cell pair 1102941

A, reconstruction of a layer III–IV border pyramid (black) and the axonal arbor of the postsynaptic basket cell (red). Note the paucity of basket cell axon in lamina IV, which is accentuated by a relatively dense terminal arbor in layer V. *B*, for clarity of display, the pyramidal axon and the basket cell dendritic tree have been shifted towards the right. *C*, after omitting non-contacting pyramidal cell axon branches (asterisks), it is apparent that the synaptic contacts arose from two ascending side branches, which, in turn, originated from the first pyramidal cell axon collateral. *D*, the presynaptic pyramidal cell collaterals established two equidistantly located *en passant* synaptic junctions (1 and 2) with two different basket cell dendrites. *Ea*, averaged pyramidal cell action potential. *Eb*, pyramidal cell activity elicited short-latency, fast-rising EPSPs in the coupled basket cell. Superimposed consecutive single sweeps. *Ec*, averaged EPSP, the decay of which could be adequately fitted with a single exponential. Note the monoexponential decay of the late phase having a similar time constant to that of the evoked events. *Ed* and *e*, when depolarized close to firing threshold, basket cell discharge could be evoked by single pyramidal cell action potentials. *Ef*, average of spontaneous EPSPs, which were captured during the same recording epoch. Current pulse capacitive artefacts in *Ed* have been removed.

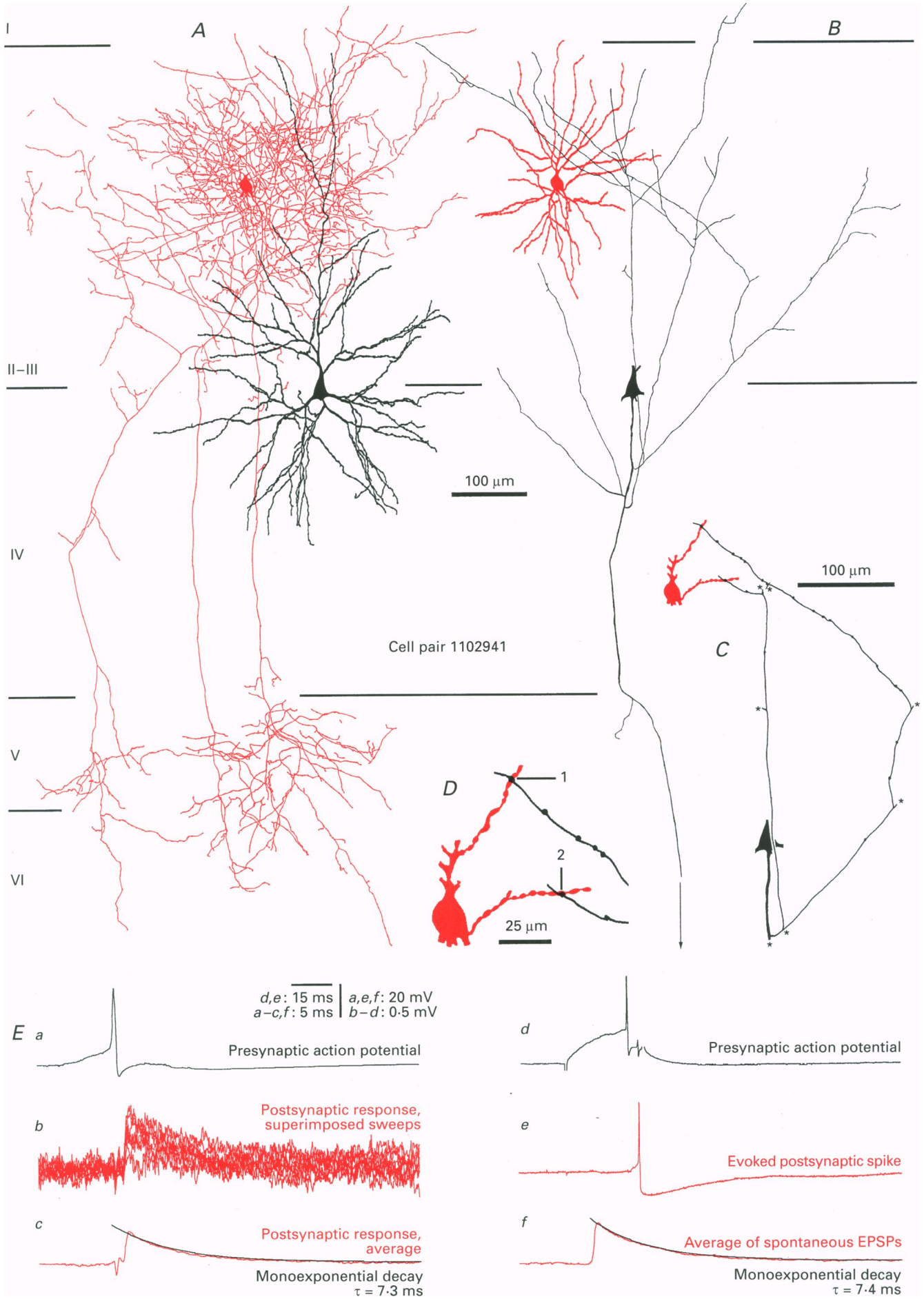
I
A
B
II–III
100 μm
IV
100 μm
Cell pair 1102941
C
V
D
1
2
VI
25 μm
E
d,e: 15 ms | a,e,f: 20 mV
a–c,f: 5 ms | b–d: 0·5 mV
a
Presynaptic action potential
b
Postsynaptic response, superimposed sweeps
c
Postsynaptic response, average
Monoexponential decay
τ = 7·3 ms
d
Presynaptic action potential
e
Evoked postsynaptic spike
f
Average of spontaneous EPSPs
Monoexponential decay
τ = 7·4 ms

inhibitory unitary connections (Buhl *et al.* 1994; Tamás *et al.* 1997), none of the presynaptic boutons established more than one synaptic junction with the postsynaptic interneurone. Eventually these data were incorporated into the respective light microscopical drawings (Figs 1*D*, 3*D*, 4*D*, 5*B* and 6*B*), while maintaining the numbering of synaptic junctions, i.e. b1 in Fig. 2*A* and *Ab* corresponds to '1' in Fig. 1*D*. These drawings therefore provide an accurate representation of the number and position of electron microscopically determined synaptic junctions. We presume that these illustrations provide the best possible estimate of the number and location of synaptic release sites, potentially barring only those axon collaterals, which, for unknown reasons, may have failed to fill with biocytin. In view of this rather stringent procedure, any possible bias of electron microscopic estimates may be therefore only in favour of underestimating the actual number of synaptic junctions.

Pyramid-to-basket cell pair 1102941. The postsynaptic basket cell gave rise to three short stem dendrites, which branched further, giving rise to a nearly spherical, compact cloud of predominantly smooth, albeit beaded, secondary and tertiary dendrites, these never terminating at a distance greater than 250 μm away from the parent cell body (Fig. 3*B*). All dendrites were contained within layers II and upper III, thus presumably largely excluding direct thalamic input to layer IV. Although most of the dense basket axon was also confined to layers II–III, three major collaterals traversed layer IV and ramified further within layer V and upper layer VI (Fig. 3*B*). The presynaptic neurone was identified as a layer III–IV border pyramidal cell, having most of its basal dendrites contained within layer IV, whereas the apical tuft of dendrites ramified predominantly in layers II–III. On its course towards the white matter the pyramidal cell axon gave rise to four collaterals, the first of them giving rise to two ascending branches which established *en passant* synaptic junctions (one each) with two basket cell dendrites. Interestingly, both contact sites were approximately equidistant (60–80 μm) from the cell body, also taking three-dimensional distortion into account (Fig. 3*D*).

Pyramid-to-basket cell pair 0812942. The postsynaptic neurone was identified as a layer III basket cell (Fig. 4*A* and *B*), having rather similar characteristics to that illustrated in the previous figure, the main difference being that no descending projection into layer V was observed. The presynaptic cell was a layer II–III pyramidal cell, being the only cell in the sample with incomplete dendritic labelling (Fig. 4*B*), probably resulting from the rapid loss of biocytin as the cell deteriorated towards the end of the recording. As this process is restricted to the somato-dendritic domain of neurones, the pyramidal axon remained very well preserved. The two branches mediating the synaptic interaction emerged from the fourth and seventh axon collateral, respectively (Fig. 4*C*), targeting the proximal portion of a basket cell primary and the distal segment of a secondary dendrite with one synaptic junction each (Fig. 4*D*).

Pyramid-to-basket cell pair 0812945. Only the most salient anatomical features of this pair of neurones have been illustrated (Fig. 5). The presynaptic layer II pyramidal cell, due to its proximity to layer I, had a very short apical tuft of dendrites and thus attained a rather stellate appearance (Fig. 5*A*). The descending pyramidal axon gave rise to nine axon collaterals, most of them ascending and forming a relatively dense local axonal arbor. One of the axon collaterals, after branching repeatedly, ascended into layer I and formed a single synaptic junction with the distal portion of a fourth order basket cell dendrite (Fig. 5*B*).

Pyramid-to-double bouquet cell pair 1412942. The neurones were reciprocally connected, with their characteristic features being described in the accompanying paper (Tamás *et al.* 1997). The presynaptic pyramidal cell innervated the double bouquet cell with two ascending axon collaterals, both originating from a proximal branch of the main axonal trunk (Fig. 6*A*). One of the collaterals established two and three synaptic junctions, respectively, close to the origin of two primary dendrites, whereas the second collateral made one synaptic junction on the cell body and, in close proximity, a second synaptic contact with a main dendrite (Fig. 6*B*). Thus, in addition to the cell body, a total of three dendritic segments were targeted. Note that similar to the previously described pyramid-to-dendrite targeting cell pair, none of the seven contact sites was separated from the cell body by a distance of more than 25 μm.

Figure 4. Pyramid-to-basket cell pair 0812942

A, reconstruction of a basket cell soma and dense axonal arbor (red) which was largely confined to the upper half of layers II–III. The presynaptic pyramidal cell dendritic arbor (black) is incompletely visualized due to the loss of biocytin. *B*, the pyramidal cell axon gives rise to the densest projection of ascending collaterals in our sample. *C*, following omission of non-contacting branches (asterisks) it is apparent that both synaptic contacts originated from the fourth and seventh primary axon collateral, respectively. *D*, each of the two connecting branches established a single, electron microscopically verified, *en passant* synaptic junction (1, 2) with the shaft of a primary and a secondary basket cell dendrite. Note the proximo-distal difference in the placement of release sites. *Ea*, averaged pyramidal cell action potential. *Eb*, single superimposed consecutive postsynaptic responses. *Ec*, averaged postsynaptic response with monoexponential decay. *Ed*, on average, spontaneous EPSPs were of comparable amplitude and showed decay kinetics similar to evoked events.

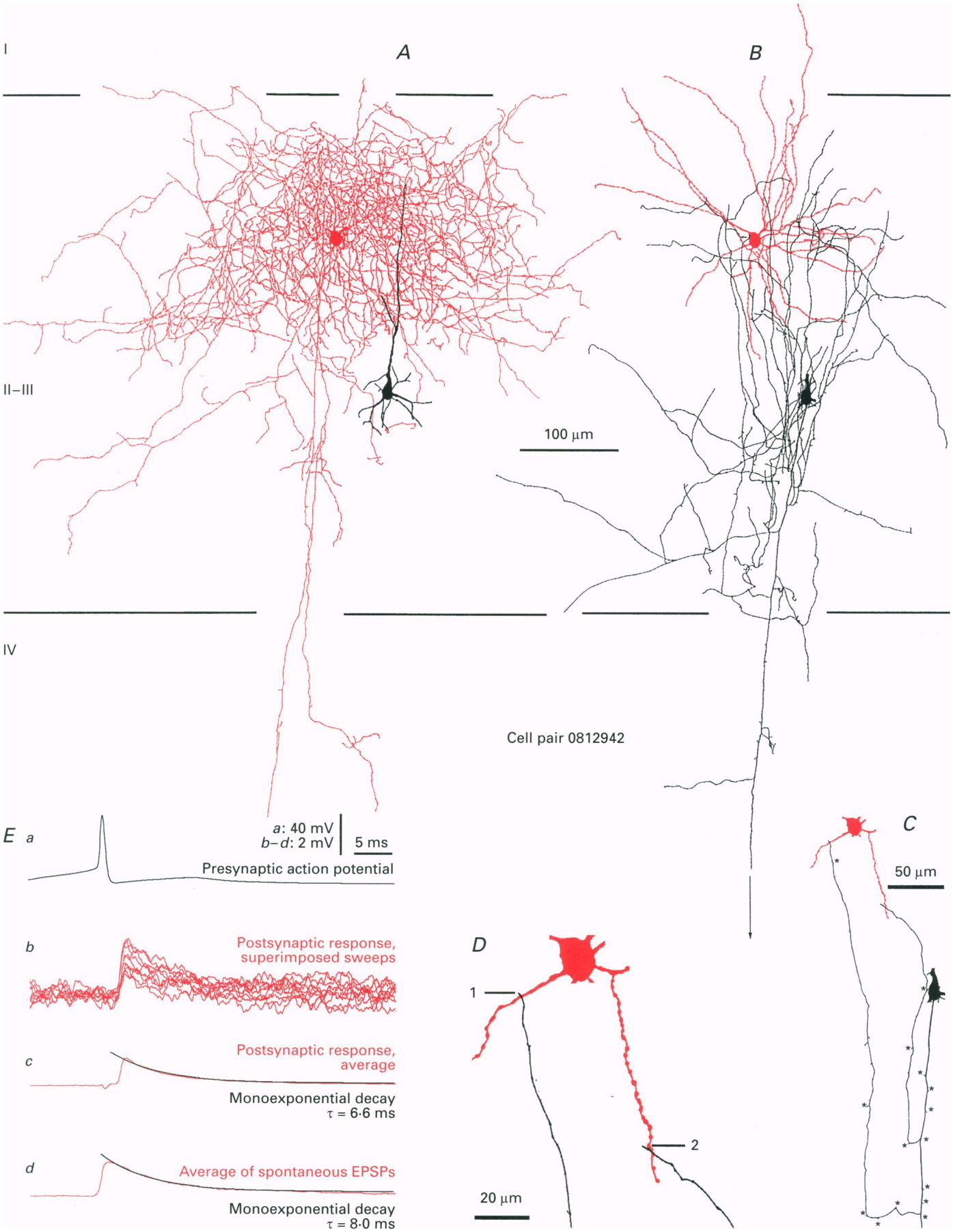

Figure 4. For legend see facing page.

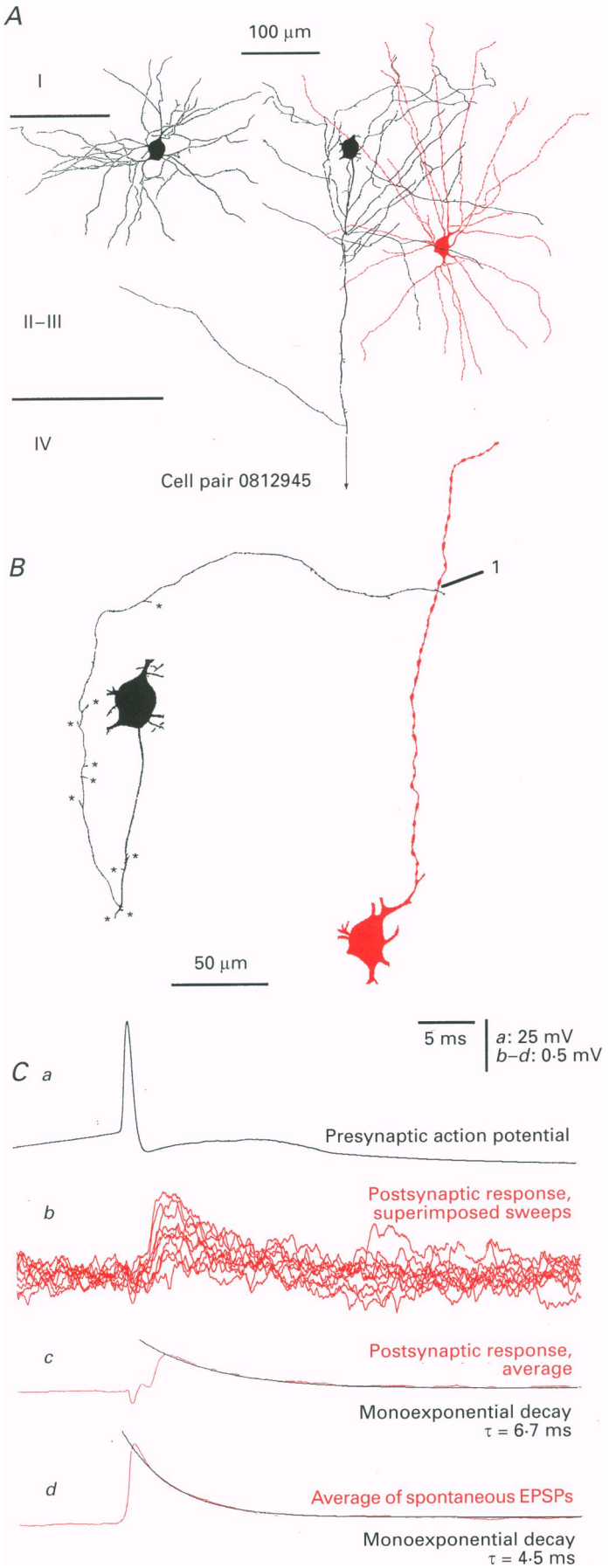

Figure 5. Pyramid-to-basket cell pair 0812945

A, reconstruction of presynaptic pyramidal cell (black; dendritic arbor shifted to the left) which had no appreciable apical dendritic tuft due to its position near the layer I–II border. The basket cell had a radially elongated dendritic arbor (red) and a very dense, compact axonal arbor (not shown), similar to the one shown in Fig. 4. *B*, when omitting non-contacting branches (asterisks), it is apparent that a daughter branch of the third pyramidal cell axon collateral forms a single, electron microscopically verified, *en passant* synaptic contact site with the distal portion of an ascending basket cell dendrite. *Ca*, averaged pyramidal cell action potential. *Cb*, superimposed, successive pyramidal cell-evoked EPSPs in postsynaptic basket cell. *Cc*, the averaged postsynaptic response had a mean amplitude of 364 μV and decayed monoexponentially back to baseline. *Cd*, spontaneous events were, on average, of larger amplitude (789 μV), having similar decay, but appreciably faster rise (~35%) parameters.

An additional layer II–III double bouquet cell (code 0409964) could be shown to receive recurrent excitatory input from a neighbouring layer II–III pyramidal neurone. Random electron microscopic bouton sampling ($n = 10$) indicated that the double bouquet axon formed the majority of synaptic junctions with dendritic spines (70%) and, to a lesser extent, with dendritic shafts (30%). Single pyramidal cell action potentials evoked a short-latency fast EPSP with

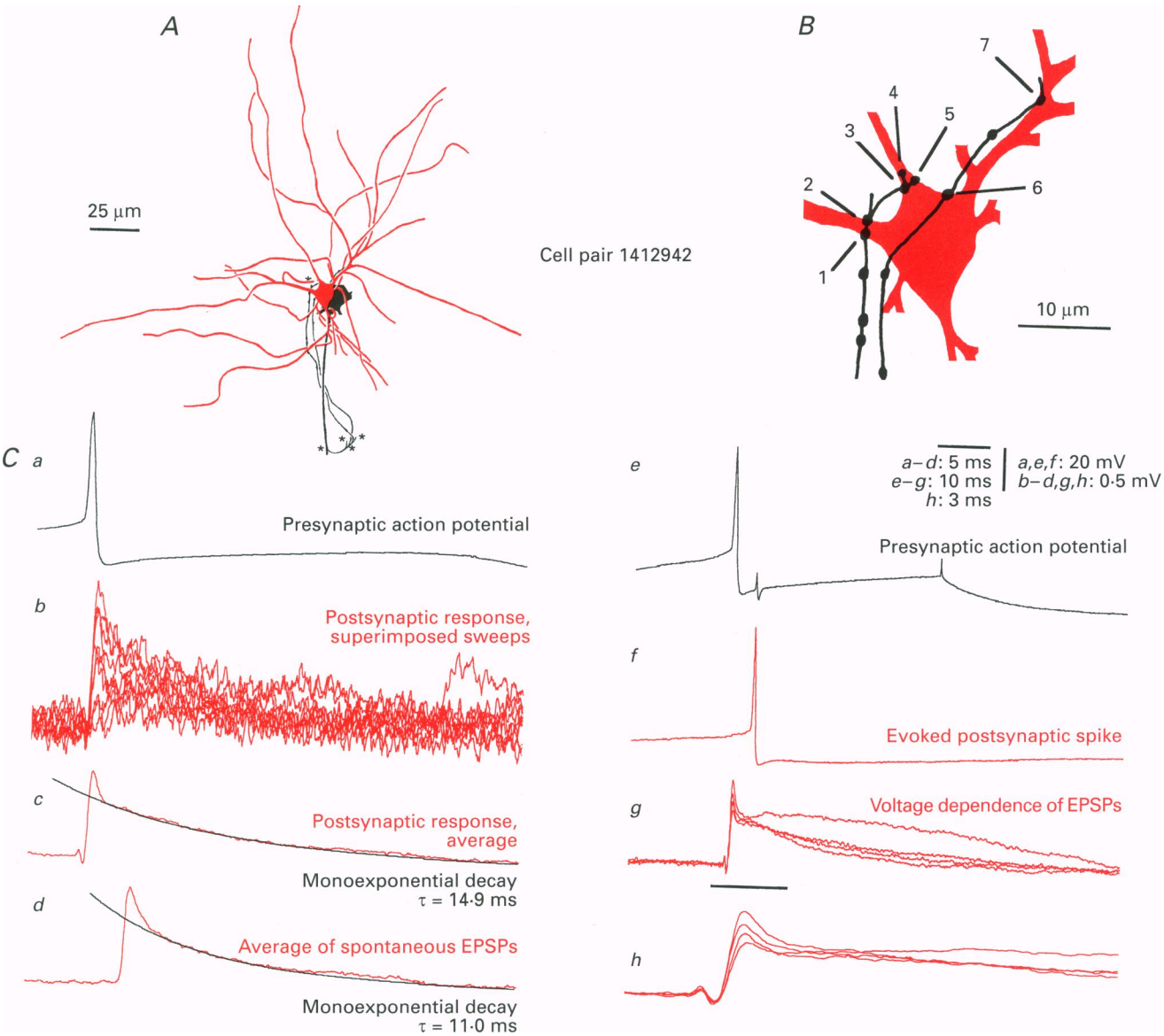

Figure 6. Pyramid-to-double bouquet cell pair 1412942

A, reconstruction of a synaptically coupled pyramidal (black) and double bouquet cell (red) pair. Only the connecting pyramidal cell axon is shown (for full reconstruction of this reciprocal interaction see Tamás *et al.* 1997). Both connecting branches originated from the first pyramidal cell axon collateral. *B*, the synaptic boutons originating from these branches were arranged in two groups (1, 2 and 3–5); the second collateral established a bouton on a third dendrite and another on the cell body near the base of the same dendrite. All synaptic junctions occupied very proximal positions. *Ca*, averaged pyramidal cell action potential. *Cb*, superimposition of successive postsynaptic responses indicates a large degree of amplitude variability. *Cc*, averaged EPSP with exponential fit of late decay. *Cd*, similar sized average of spontaneous EPSPs, showing decay kinetics similar to evoked events. *Ce* and *f*, at depolarized membrane potentials, the effect of pyramidal cell discharge could be sufficient to trigger single action potentials in the postsynaptic double bouquet cell. *Cg*, superimposed averages of pyramidal cell-evoked EPSPs at 4 different membrane potentials (−50, −55, −65 and −79 mV). Note the prolonged EPSP at the most depolarized holding potential. *Ch*, averages shown in *Cg* on an expanded time scale (time window indicated by horizontal bar). Concomitant with membrane depolarization the early phase of postsynaptic responses showed a successive decrease in their average amplitudes.

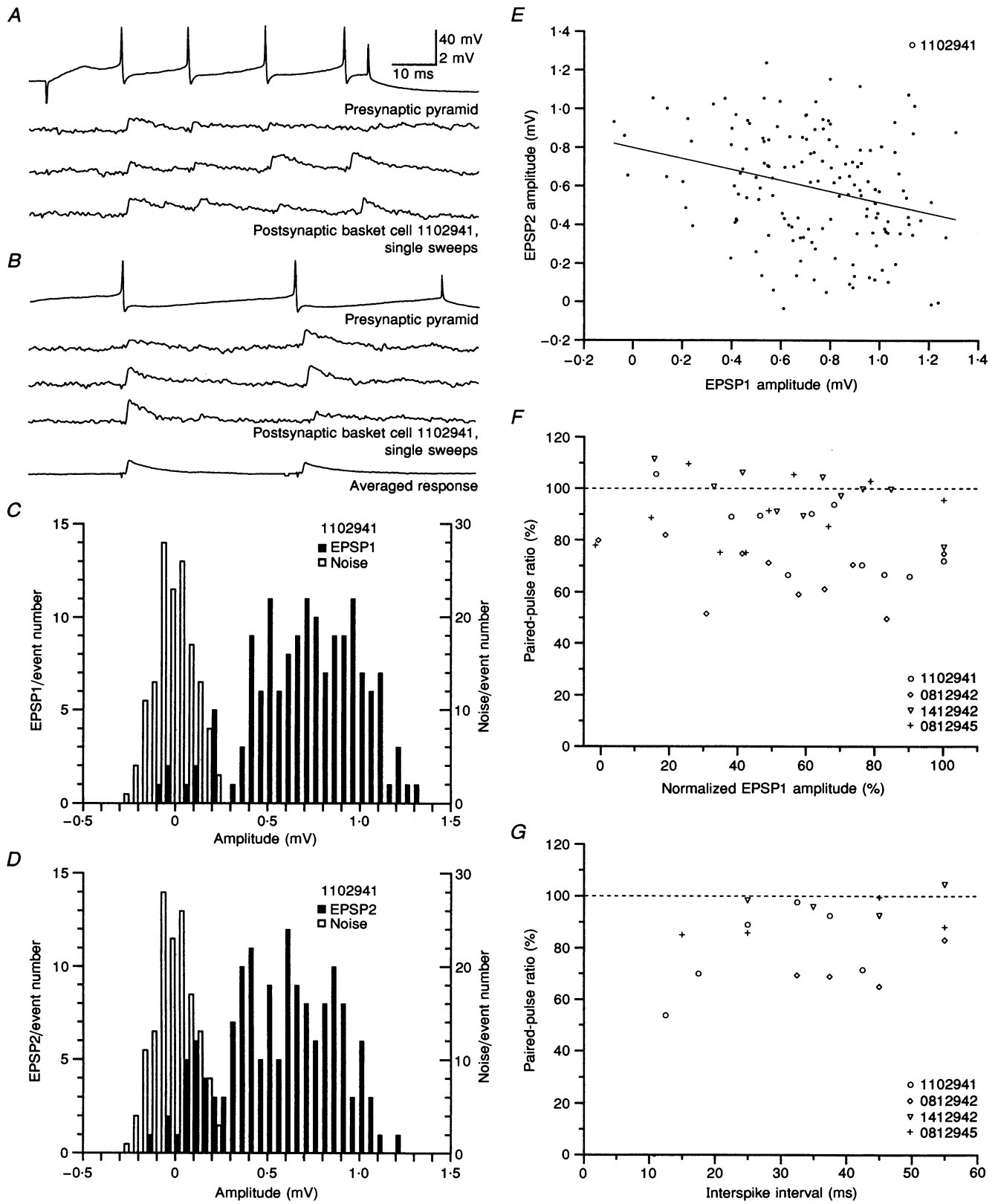

Figure 7. Paired-pulse modulation of unitary pyramid/interneurone EPSPs

A, brief trains of presynaptic action potentials could elicit variable postsynaptic response patterns, ranging from a successive decline in EPSP amplitude to a gradual increase in response magnitude or could be without a consistent tendency. *B*, when applying the paired-pulse protocol (same cell pair as in *A*, but adjusting pulse duration and current intensity so as to elicit only 2 action potentials), the analysis of single

a 10–90% rise time of 1·4 ms, an average amplitude of 218 μV and, when measured at half-amplitude, a duration of 4·1 ms. Unfortunately, however, the loss of biocytin from the interneurone dendrites prevented the analysis of the location and number of synaptic junctions and this cell pair was therefore not included in the sample ($n = 5$) of fully characterized interactions.

Physiological properties of unitary pyramid-to-interneurone EPSPs

The postsynaptic interneurones had a mean resting membrane potential of $-67·6 \pm 6·9$ mV, an input resistance of 51 ± 15 MΩ and an average membrane time constant of $9·2 \pm 8·5$ ms. For the respective interactions, averages of postsynaptic effects were obtained at membrane potentials ranging from −60 to −79 mV (mean, $-70·0 \pm 8·4$ mV). The amplitudes of averaged unitary EPSPs (including postsynaptic response failures) varied between 359 and 1657 μV, with a mean of 1005 ± 518 μV. Generally, the amplitudes of averaged spontaneous EPSPs (captured during the same epoch and at the same membrane potential) were similarly sized, ranging from 635 to 1652 μV, although these measurements may have been biased towards larger events (> 300 μV), with an unknown proportion of smaller EPSPs being obscured by the recording noise. In two recordings, measurements of postsynaptic effects were obtained at three or four different holding potentials, varying between −90 and −65 mV, and −79 and −50 mV (Fig. 6*Cg* and *h*), respectively. In both instances depolarization of the membrane potential resulted in a concomitant, fairly linear decrease of the response amplitude, ranging from 798 to 626 μV and 1018 to 644 μV (Fig. 6*Cg* and *h*), respectively.

In comparison with rat neocortical pyramid-to-pyramid EPSPs (Mason *et al.* 1991; also determined at rather hyperpolarized membrane potentials), the duration of unitary pyramid-to-interneurone EPSPs in the cat was generally brief. The duration of the EPSP, measured at half-amplitude, varied between 2·9 and 5·7 ms, with a mean of $4·7 \pm 1·0$ ms. Spontaneous EPSPs had an average duration of $4·7 \pm 1·7$ ms, ranging from 3·2 to 7·3 ms, which compares well with the evoked EPSPs. At hyperpolarized membrane potentials, the decay of evoked and spontaneous EPSPs could be generally well fitted with a single exponential function (Figs 1*Ed* and *e*, 3*Ec* and *f*, 4*Ec* and *d*, 5*Cc* and *d*, and 6*Cc* and *d*). Unitary EPSPs decayed with an average time constant of $7·8 \pm 4·3$ ms (range, 3·4–14·9 ms), the mean of spontaneous events being very similar ($7·0 \pm 2·8$ ms, varying from 4·3 to 11·0 ms). When comparing the decay time constants of unitary EPSPs with the corresponding membrane time constants (range, 4·2–22·9 ms), it was apparent that they were very similar, their mean ratio being $1·0 \pm 0·3$. Thus it appears that, at hyperpolarized membrane potentials, the decay of EPSPs in cortical interneurones is largely shaped by passive membrane properties. This notion, however, does not necessarily apply at more depolarized membrane potentials, since in the pyramid-to-double bouquet cell pair the decay of the EPSP was greatly prolonged when depolarizing the postsynaptic neurone close to the action potential threshold (Fig. 6*Cg*).

All unitary pyramid-to-interneurone EPSPs were characterized by fast 10–90% rise times, which were, on average, $0·67 \pm 0·25$ ms. In view of the fact that in two instances (1612941 and 1412942) all release sites were placed proximally, i.e. close to the soma (< 40 μm), whereas in the remainder of cases they were located in either intermediate positions (1102941 and 0812942) or very distally (0812945), it is conceivable that the differential placement of synaptic contact sites may affect the very fast EPSP rise times, due to different degrees of electrotonic attenuation. The relation, however, between the placement of the synaptic sites on the somato-dendritic axis and the rise time was not very prominent. Moreover, the rise times of averaged spontaneous EPSPs ($0·68 \pm 0·18$ ms), presumably originating from various parts of the dendritic tree, were similar to those evoked at known sites by identified pyramidal cell input. Conversely, however, we cannot exclude the possibility that electrotonic attenuation may have differentially reduced the amplitude of at least some distally originating spontaneous EPSPs below detection threshold, therefore resulting in a skew of their rise time distribution towards faster events.

events revealed no obvious tendency in the short-term modulation of response amplitudes. However, averaging of successive events made it apparent that the conditioning pre-pulse/first EPSP resulted in a relatively small reduction of the mean second EPSP amplitude. *C* and *D*, the tendency towards an overall decrease in the amplitude of second EPSPs was also apparent in amplitude histograms of first and second EPSPs, respectively. Note the overall shift of second EPSP measurements towards smaller amplitudes and the greater proportion of events overlapping the distribution of concomitantly measured recording noise, an indication of a greater number of postsynaptic response failures. *E*, same cell as illustrated in *A–D*. A scatter plot of first EPSP amplitudes *versus* those of the successive second EPSP revealed an apparent interdependence, showing an inverse correlation (linear regression; $r = 0·28$, $P < 0·05$) of first and second EPSP, i.e. large first events were more frequently followed by small second events, and vice versa. *F*, to minimize the influence of recording noise, events were sorted with respect to their amplitude, binned (10% of events per bin) and averaged. Subsequently normalized first EPSP amplitudes were plotted against the respective paired-pulse ratios. Generally the paired-pulse ratios of binned trials indicated the presence of paired-pulse depression (i.e. data points were below dashed line), even for small EPSP1 amplitudes. Although several values were > 100%, this difference never reached statistical significance. *G*, when plotting paired-pulse ratios against interstimulus intervals, depression was observed at all tested intervals and appeared to be more prominent at shorter intervals.

Table 2. Data for EPSPs subjected to quantal analysis

Cell pair	Target	RMP (mV)	R_i (MΩ)	n	Events	σ_{noise} (μV)	μ_{EPSP} (μV)	σ_{EPSP} (μV)	Rise time (ms)	Half-width (ms)	Decay τ (ms)
0812945	BC	−71	37	1	652	124	316	219	1·00	5·4	6·7
1102941	BC	−64	55	2	675	84	388	244	0·48	5·4	7·4
0812942	BC	−78	62	2	700	275	1224	495	0·78	4·9	6·6
1612941	DTC	−61	33	5	468	84	891	695	0·74	2·9	3·4
1412942	DBC	−64	66	7	498	96	709	450	0·39	5·1	14·9

Target: BC, basket cell; DTC, dendrite-targeting cell; DBC, double bouquet cell. RMP, resting membrane potential of postsynaptic interneurone; R_i, input resistance of postsynaptic interneurone; n, number of synaptic junctions verified with electron microscopy; Events, number of EPSPs analysed; σ_{noise}, S.D. of noise; μ_{EPSP}, mean amplitude of EPSP; σ_{EPSP}, S.D. of EPSP; Rise time, 10–90% rise time of EPSP; Half-width, duration of EPSP at half-peak amplitude; Decay τ, decay time constant of EPSP.

Paired-pulse modulation of pyramid-to-interneurone EPSPs

When trains of action potentials were evoked in presynaptic pyramidal cells, the postsynaptic responses showed a relatively large degree of variability, ranging from a gradual decrease in amplitude to a decremental increase or seemingly random fluctuation of the response magnitude (Fig. 7*A*). To systematically investigate the effect of the occurrence of a presynaptic action potential on subsequent evoked responses, we employed a paired-pulse protocol, by adjusting the current pulse to eliciting *only* two presynaptic action potentials (Fig. 7*B*). Such data were obtained in four of the connections (basket cell pairs 1102941, 0812942 and 0812945 and the double bouquet cell pair 1412942) with the number of events ranging from 147 to 436. In all presynaptic cells, pairs of action potentials were elicited by a single current pulse of 100–200 ms duration at a rate of 1 Hz. Interspike intervals were varied by adjusting the current intensity and ranged from 10 to 60 ms.

Although individual trials appeared to show no obvious tendency, the mean of all *averaged* second EPSPs was 84 ± 12% (range, 68–98%) of the respective conditioning first events, thus indicating the predominance of paired-pulse depression at pyramid-to-interneurone connections (Fig. 7*B*). All three pyramid-to-basket cell pairs showed statistically significant paired-pulse depression (80 ± 11%; Mann–Whitney U test; $P < 0·05$), whereas the paired-pulse protocol left synaptic transmission at the pyramid-to-double bouquet cell connection virtually unaffected (98%; Mann–Whitney U test; $P > 0·05$). The overall decrease of the average amplitudes was not accompanied by a change of the measured response variability (mean of averaged first EPSPs 0·79 ± 0·38 *vs.* 0·66 ± 0·38 mV for second EPSP). This tendency was also apparent when constructing amplitude histograms, which showed a general shift of the distribution towards smaller amplitudes and a greater overlap with the noise measurements, suggesting a larger proportion of postsynaptic response failures (Fig. 7*C* and *D*). No attempt was made to extract the quantal parameters of the respective distributions, due to the limited number of events (< 200) at any given interspike interval.

When the amplitudes of second EPSPs were plotted against those of the preceding events, a statistically significant negative correlation was found in two of the interactions ($P < 0·05$; Pearson's r table, Fig. 7*E*; pairs 1102941 and 1412942). The correlation coefficients (r) for these pairs were −0·28 ($n = 147$ observations) and −0·15 ($n = 244$), respectively. In the remaining two connections, there was no significant correlation between first and second EPSPs ($P > 0·05$). However, with the degree of correlation between successive events being also influenced by the recording noise variance, we sought to minimize the influence of this parameter by comparing averages of presorted events. Single sweeps were sorted with respect to the amplitude of the first EPSP and separated into ten groups, each group containing 10% of all measured events. For the four measured interactions the averaged largest 10% of first events were in the range 161–214% of the average of all first EPSPs. Second EPSP amplitudes were then measured and averaged for each 10% group, e.g. all second EPSPs following the 10% of preselected largest first events. Finally, for each of the ten groups the corresponding paired-pulse ratio was calculated, here taken as the ratio of averaged second EPSP and the mean conditioning EPSP (i.e. the average of *all* first EPSPs) × 100. A value > 100 (Fig. 7*F*) would then indicate the presence of paired-pulse facilitation, i.e. the second EPSP amplitude exceeding that of the mean conditioning first EPSP. Finally, to facilitate comparison of the individual cells with respect to differences in the amplitude distributions of the conditioning first EPSPs, the data were normalized by setting the average amplitude of the largest 10% of first events as 100%.

These results are illustrated in a scatter plot (Fig. 7*F*), showing that for all pyramid-to-basket cell pairs the majority of data points were below the dashed line, thus indicating the overall predominance of paired-pulse depression. Although in several instances the calculated paired-pulse ratios exceeded 100%, it never reached

statistical significance, when comparing the respective group of preselected events with all second EPSPs (Mann–Whitney U test; $P > 0{\cdot}05$). Interestingly, as indicated above, there was only a statistically significant negative correlation between second EPSP amplitudes and the magnitude of preceding events in two cells. In any of the connections, even for very small first events, statistically significant paired-pulse facilitation was never observed. Conversely, very large conditioning EPSPs (10% largest first events) resulted in only one of the cells (1412942) in a statistically

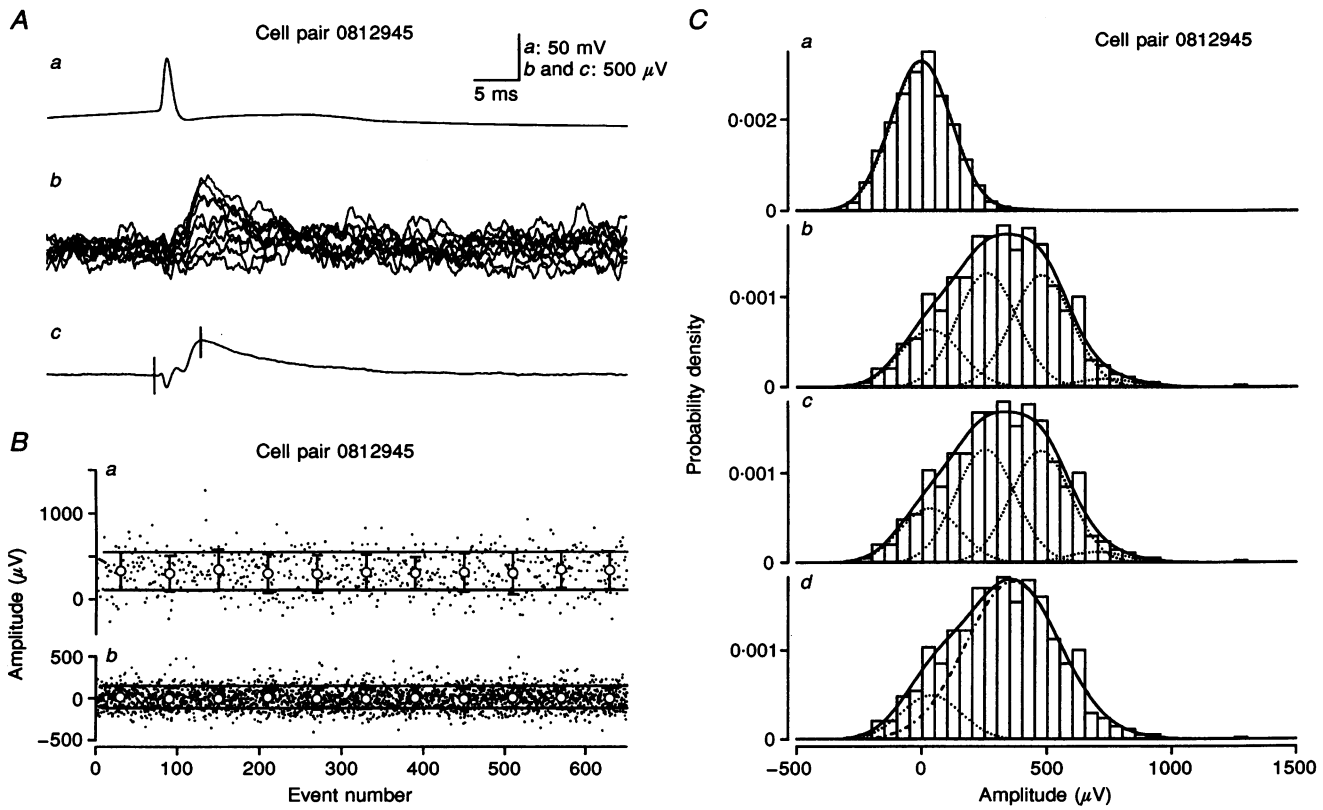

Figure 8. Amplitude fluctuations of evoked EPSPs in a connection with a single synaptic junction

Aa, average of presynaptic action potentials ($n = 652$). All synaptic events were aligned on the rising phase of the presynaptic action potential. *Ab*, single successive sweeps of EPSPs recorded from a basket cell evoked by an action potential in the presynaptic pyramidal cell ($n = 10$). *Ac*, average of all EPSPs used for quantal analysis for this cell pair ($n = 652$). The cursor setting for amplitude measurements is indicated by the two vertical lines. *Ba*, plot of EPSP amplitude *versus* event number with cursor settings as indicated in *Ac*. The means and S.D. values of blocks of 60 consecutive events are shown as open circles with error bars. The horizontal lines indicate the mean ± S.D. for the first 60 events. *Bb*, corresponding noise measurements obtained from the baseline period immediately preceding each event. Four noise measurements were made for each event ($n = 2608$). The means and S.D. values of blocks of 240 consecutive events are shown as open circles with error bars, with the horizontal lines showing the mean ± S.D. for the first 240 events. *Ca*, amplitude frequency histogram of the noise scaled as a probability density with the best fitting sum of two Gaussian functions superimposed. The means of the two Gaussian functions were −1 and 420 μV and the respective weights were 0·99 and 0·01. This double Gaussian function served as the noise distribution during deconvolution. *Cb*, amplitude frequency histogram of the EPSP scaled as a probability density with the best-fitting sum of double Gaussian functions superimposed. Three double Gaussian functions were necessary in addition to the failure peak. The double Gaussian functions had variances as determined from the noise in *Ca*. *Cc*, amplitude frequency histogram of the EPSP scaled as a probability density with the best-fitting quantal model without quantal variance superimposed. Three components were necessary in addition to the failure peak. This model was not significantly different from the model in *Cb* ($P > 0{\cdot}05$; Wilks statistic). *Cd*, amplitude frequency histogram of the EPSP scaled as a probability density with the best-fitting quantal model with quantal variance superimposed. Only one component was necessary in addition to the failure peak. This model was not significantly different from the model in *Cb* ($P > 0{\cdot}05$; Wilks statistic). The parameters for the quantal models are given in Table 3. Bin size for the histograms in *C*, 50 μV. Dotted lines indicate double Gaussian functions determined from the noise; dashed and dotted line indicates a component with quantal variance, and the continuous lines represent the sum of the components.

Table 3. Estimated parameters for quantal models

			Unconstrained		Quantal model				Quantal model with variance				
Cell pair	n	m	$k-1$	llh	$k-1$	q (μV)	Offset (μV)	llh	$k-1$	q (μV)	Offset (μV)	c.v.	llh
0812945	1	1	3	−4437·8	3	222 ± 19	32 ± 33	−4437·9	1	327 ± 29	37 ± 32	0·45 ± 0·07	−4438·6
1102941	2	2	4	−4656·8	4	228 ± 16	27 ± 20	−4657·8	2	260 ± 45	9 ± 89	0·46 ± 0·07	−4658·6
0812942	2	2	3	−5335·7	3	557 ± 48	72 ± 134	−5335·9	2	652 ± 114	51 ± 262	0·34 ± 0·10	−5336·6
1612941	5	4	9	−3691·0	9	353 ± 20	−10 ± 36	−3690·3	4	656 ± 30	−23 ± 24	0·38 ± 0·04	−3650·9
1412942	7	4	8	−3714·8	8	227 ± 10	37 ± 15	−3718·5	4	362 ± 42	39 ± 21	0·33 ± 0·10	−3723·1

n, number of release sites; m, number of somato-dendritic segments innervated; k, number of components; llh, log likelihood; q, apparent quantal size; Offset, failure-peak offset from zero; c.v., quantal coefficient of variation.

significant smaller second EPSP, when comparing the respective group of preselected events with all second EPSPs (Mann–Whitney U test; $P < 0·05$).

Since previous work using the paired-pulse protocol has indicated that the interval between the conditioning first event and the successive test stimulus may also affect the degree of paired-pulse modulation (for review see Zucker, 1989), a similar comparison was made by pooling the data with respect to the temporal spacing of action potentials in the presynaptic pyramidal cells. Individual sweeps were sorted with respect to the interspike interval, binned and averaged. Paired-pulse ratios were determined as described above and plotted against the respective interspike intervals (Fig. 7*G*). It was apparent that paired-pulse depression predominated at all intervals. With one exception, there was no marked effect of interspike interval on the magnitude of the second event. Only in the basket cell pair 1102941 at very short intervals, a significantly (10–15 ms; $P < 0·05$; Mann–Whitney U test) greater degree of paired-pulse depression was observed. For the remainder of data there was no appreciable effect of interspike interval on the degree of paired-pulse depression.

Amplitude fluctuations of EPSPs

The amplitude of the evoked EPSPs fluctuated from trial to trial (Fig. 8*A*). The variance of the EPSP amplitude in all five connections exceeded that of the noise. In order to test whether the amplitude fluctuations reflected quantal variation of the EPSPs, a quantal analysis by noise deconvolution was carried out. To this end, epochs were selected for which the averaged EPSP amplitude remained stationary. An example of an EPSP amplitude monitored over time is shown in Fig. 8*Ba*, and corresponding noise amplitudes in Fig. 8*Bb*. The number of EPSP amplitude measurements for each connection obtained during stationary recording conditions ranged between 468 and 700. Ensemble data for these epochs are given in Table 2.

The noise could be represented as a sum of two Gaussian functions (Fig. 8*Ca*). For none of the cells could the quantal models be rejected against the fully unconstrained alternative ($P > 0·05$; Wilks statistic). A quantal model is therefore an adequate description of the amplitude fluctuations. For all five EPSPs, the minimum number of components of the quantal model with quantal variance was smaller than the minimum number of components of the corresponding models without quantal variance. The estimated quantal coefficient of variation in this quantal model with variance ranged between 0·33 and 0·46. The quantal models with the minimum number of components determined in this way, without and with quantal variance, are illustrated in Fig. 9 for all five connections. The corresponding parameter estimates are summarized in Table 3. Introducing quantal variance reduced the minimum number of components necessary to produce an acceptable fit, concomitant with an increase in the estimated quantal size. Note also that the standard error of the estimates in most instances is larger in the quantal model with variance than in the quantal model without variance.

The smallest number of double Gaussian functions for the models without quantal variance, excluding the failure peak (i.e. $k - 1$; Table 3), exceeded the electron microscopically determined number of synaptic junctions for all five connections. In contrast, when quantal variance was included in the model, the smallest number of components, excluding the failure peak, was either the same as, or smaller than, the electron microscopically determined number of synaptic contacts for all five connections. This result was obtained also for the connection (cell pair 0812945; Fig. 5) where only one synaptic contact was detected during the electron microscopic examination. Thus, for all three pyramid-to-basket cell connections, for the quantal model with variance, the smallest number of components coincided with the anatomically determined number of synaptic junctions. For the pyramid-to-dendrite-targeting cell connection (1612941; Figs 1 and 2) and the pyramid-to-double bouquet cell connection (1412942; Fig. 6), the minimum number of components was less than the number of synaptic junctions. Any model with a larger number of components would also be statistically compatible with the data. A larger number of

components would generally lead to better fits with smaller quantal size accompanied by smaller quantal variation. Thus, the estimates given for the quantal model with variance in Table 3 represent maximum estimates for quantal sizes and quantal variation. For example, for the pyramid-to-double bouquet cell connection with seven synaptic junctions (cell pair 1412942; Fig. 6) a quantal model with variance, incorporating seven components in addition to the failure peak, gave a slightly better fit (log likelihood, −3720·0), with a smaller estimated quantal coefficient of variation (0·12 ± 0·09) and a smaller estimated quantal size (246 ± 18 μV). The fit, however, was not significantly better than the fit of the model with four components in addition to the failure peak ($P > 0·05$; Wilks statistic).

In order to gain insight into the rules of transmitter release at these synapses, we tested whether a binomial type process could account for the data. The binomial parameter n was assumed to reflect the number of release sites. As it was necessary to incorporate a significant amount of variance

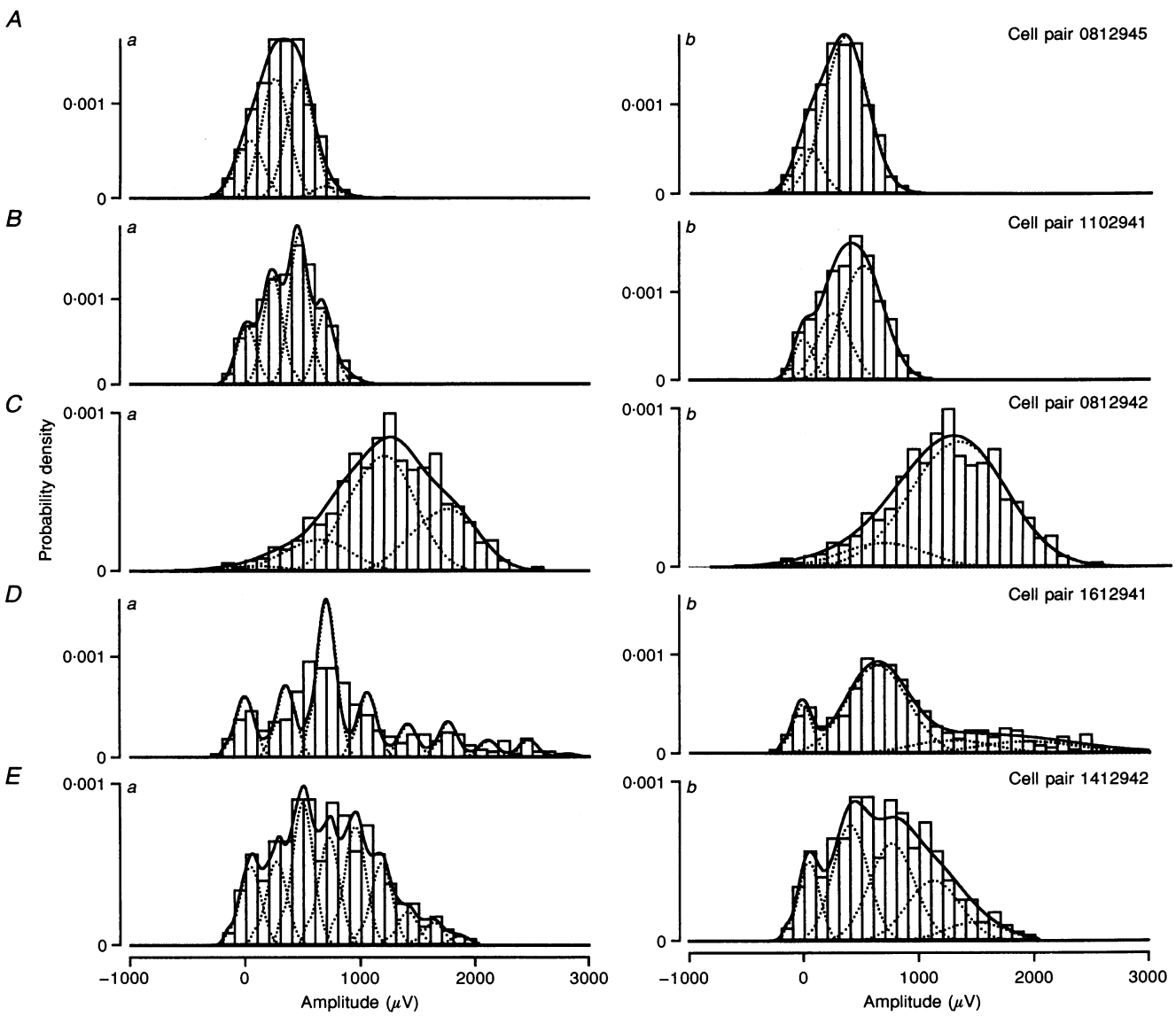

Figure 9. Amplitude distributions for all five connections

Amplitude frequency histograms scaled as probability densities for all 5 connections with fitted quantal models superimposed. The number of EPSP amplitudes analysed are given in Table 2. The estimated quantal parameters are shown in Table 3. To the left (*Aa*, *Ba*, *Ca*, *Da* and *Ea*), a quantal model without quantal variance has been fitted to each probability density function. To the right (*Ab*, *Bb*, *Cb*, *Db* and *Eb*), a quantal model including quantal variance has been fitted to each probability density function. The summed distribution (continuous line) as well as the individual components (dotted lines) are shown. Note that some of the components have very small weights. The histograms and fitted distributions in *Da* and *b* have been truncated at 3000 μV, therefore omitting the display of four events exceeding 3000 μV for this connection. Bin size for the histograms, 100 μV.

Table 4. Estimated parameters for compound binomial model

Cell pair	n	q (μV)	Offset (μV)	c.v.	P_1	P_2	P_3	P_4	P_5	P_6	P_7	llh	P_{binomial}
0812945	1	327	37	0·45	0·85	—	—	—	—	—	—	−4438·6	—
1102941	2	284	−11	0·40	0·73	0·73	—	—	—	—	—	−4661·1	0·03
0812942	2	802	−276	0·28	0·94	0·94	—	—	—	—	—	−5336·8	0·71
1612941	5	696	−39	0·44	0·84	0·12	0·12	0·12	0·12	—	—	−3666·8	<0·01
1412942	7	395	32	0·38	0·44	0·43	0·43	0·42	0·00	0·00	0·00	−3724·2	0·54

n, number of release sites; q, apparent quantal size; Offset, failure-peak offset from zero; c.v., quantal coefficient of variation; P_n, release probabilities for each of n sites; llh, log likelihood; P_{binomial}, significance probability obtained in Wilks test for the compound binomial model tested against the quantal model with variance.

into the unconstrained model in order for the number of components, excluding the failure peak, not to exceed the electron microscopically determined number of synaptic junctions, we incorporated quantal variance in the binomial release models as well. Two types of models were tested: a uniform binomial process for which all the probabilities (P_n) were equal and a non-uniform (compound) binomial process where all the probabilities could be varied. The maximum likelihood estimates for the compound binomial model are given in Table 4. The estimated offset of −276 μV for cell pair 0812942 is probably due to an outlier in the probability density function, which may occur with a low frequency of failures, which was the case for this EPSP. This again makes the estimate for the quantal size unreliable, and the quantal size is therefore likely to be an overestimate for this EPSP. For two of the cells (1102941 and 1612941) the binomial model was rejected in favour of the quantal model with variance and no constraints on the amplitude probabilities ($P < 0·05$; Wilks statistic). For the two other connections with more than one release site, the binomial model could not be rejected, and should therefore be accepted as an adequate description of the amplitude fluctuations. The compound binomial model was reduced to a uniform binomial model by the fitting algorithm for these two connections, with n reassuringly consistent with the number of components in the unconstrained quantal variance model and for one of the pyramid-to-basket cell connections (0812942; Fig. 4) also in agreement with the electron microscopic evidence for two synaptic junctions. For the pyramid-to-double bouquet cell connection with seven synaptic contacts detected during the electron microscopic analysis (1412942; Fig. 6), a binomial model with $n = 4$ was obtained, consistent with the minimum number of components for the unconstrained quantal model with variance. In contrast, the amplitude fluctuations for the pyramid-to-dendrite-targeting cell connection with five synaptic junctions (1612941; Figs 1 and 2) and one of the pyramid-to-basket cell pairs (1102941; Fig. 3) were inconsistent with a binomial model. Thus, whereas the binomial model could adequately account for the amplitude fluctuations in two of the junctions, it failed to fit the other two with more than one release site.

DISCUSSION

Dual intracellular recordings of synaptically coupled pairs of neurones have been employed to investigate recurrent pyramidal cell feedback to inhibitory local-circuit neurones of the cat visual cortex. Following their physiological characterization, the anatomical correlate of a total of five pyramid-to-interneurone interactions was fully reconstructed, using a correlated light and electron microscopic approach. Since light microscopic counts of putative contact sites are a rather poor indicator of the exact number of *synaptic junctions* (Tamás *et al.* 1997) we considered the electron microscopic verification of all light microscopically predicted sites of membrane apposition between pre- and postsynaptic elements as essential to arrive at the best possible estimate of the number of release sites. Due to this stringent and rather time-consuming procedure our sample is relatively small, although it represents the most comprehensive analysis as yet of cortical connections with known numbers of synaptic junctions. Since we encountered only two postsynaptic interneurones other than basket cells it is, at present, necessary to treat morphologically diverse local-circuit neurones as a broad class, using the denominator 'interneurone'. Moreover, there were no conspicuous differences in the kinetic properties of unitary EPSPs in basket cells ($n = 3$) when compared with those in other local-circuit neurones with an overall target preference for dendrites and spines ($n = 2$). However, with so few available data more work is needed to determine whether other, perhaps more subtle, differences exist in the recurrent activation of different classes of GABAergic neurones.

The anatomical and physiological substrate of unitary interactions

The electron microscopic evaluation of pyramid-to-interneurone connections in the cat neocortex indicates that

the number of synaptic junctions may vary considerably, ranging from one to seven, thus being apparently fewer when compared with the only other available data in a different neocortical area (rat somatomotor cortex: two examples with six and twelve presumed contacts, several of which were confirmed electron microscopically; Deuchars & Thomson, 1995), but appreciably more than in rat hippocampus, where recurrent feedback to interneurones appears to be mediated generally by one, and occasionally two, synaptic junctions (Gulyás, Miles, Sík, Tóth, Tamamaki & Freund, 1993; Buhl *et al.* 1994). With regard to the placement of the release sites, it appears that, across cells, they could be at virtually any part of the somato-dendritic surface. With respect to the distribution of synaptic junctions originating from individual presynaptic pyramids, however, it was apparent that the terminals providing the inputs to dendrite-targeting and double bouquet cells were clustered on a relatively small surface area of the postsynaptic neurone (for possible functional implications, see below).

All unitary EPSPs elicited in cortical interneurones were characterized by very short 10–90% rise times, which were in the same range as those measured for pyramid-to-interneurone connections in the rat sensorimotor cortex (Thomson *et al.* 1993*b*), but considerably shorter than the same measurements when obtained at pyramid-to-pyramid connections (Mason *et al.* 1991; Thomson *et al.* 1993*a*). Conceivably, for at least two of the connections, this difference may be at least partially explained by the very proximal placement of the synaptic junctions, but not for the remainder of interactions in which the synaptic junctions were placed on medium calibre or even distal dendritic segments. Similar to the rise times of evoked events, those of spontaneous EPSPs, presumably (also) originating at various distances from the cell body, had equally fast kinetics. It thus appears that the dendritic location of excitatory synapses on cortical interneurones has, in contrast to pyramidal neurones (Spruston, Jaffe & Johnston, 1994), relatively little effect on the properties of somatically recorded EPSPs, perhaps due to the electrotonic compactness of their dendrites (but see Thurbon, Field & Redman, 1994). Alternatively, it is conceivable that the kinetics of interneuronal AMPA receptors may have also affected the fast EPSP time course (Koh, Geiger, Jonas & Sakmann, 1995). Furthermore, despite the relatively negative membrane potentials, we cannot exclude the activation of voltage-gated conductances which may have facilitated the propagation of EPSPs along the dendrites and could have therefore affected somatic EPSP peak amplitude measurements (for review see Yuste & Tank, 1996). If present, however, the time course of these active conductances would have to be rather brief, since the decay of unitary as well as spontaneous EPSPs was invariably shaped by the passive membrane properties. It should be emphasized, however, that different conditions may apply, when depolarizing the membrane potential closer to firing threshold (Stern, Edwards & Sakmann, 1992), as demonstrated by the dramatic prolongation of the pyramidal cell-evoked EPSP in the postsynaptic double bouquet cell (Fig. 6*Cg*).

Both the amplitude and the time course of unitary pyramid-to-interneurone EPSPs have important implications for the processing of converging excitatory inputs. At resting membrane potentials *in vitro* such unitary pyramid-to-interneurone EPSPs were invariably ineffective in eliciting a suprathreshold response. Only when the postsynaptic interneurone was brought close to firing threshold, were single pyramidal-evoked EPSPs able to trigger action potentials (Figs 3*Ed* and *e*, and 6*Ce* and *f*). However, since, at least in our slice preparation, many interneurones are relatively hyperpolarized, several converging excitatory inputs may be required to sum up and depolarize the cell to firing threshold. In view of the very rapid decay of unitary EPSPs in interneurones, any incoming synaptic potentials can summate effectively only if they arrive with a high degree of temporal synchrony (König, Engel & Singer, 1996). Extrapolating from the time constants of EPSP decay and further assuming that the events have almost completely decayed back to baseline within a period of three time constants (mean $\tau = 7{\cdot}8$ ms; with the caveat that the somatic leak conductance associated with sharp microelectrode recordings may result in a shortening of the measured membrane time constants), it is reasonable to infer that asynchronous synaptic events separated by intervals > 25 ms show only negligible response summation. However, with the membrane time constant of interneurones being in the same range as the interspike interval of their output, they may nevertheless operate as temporal integrators, rather than coincidence detectors, at least when applying the relatively strict definition of König *et al.* (1996). Yet, the same authors also argue for coincidence detection occurring in cortical neurones on the basis that the *effective* time constant which determines the integration of synaptic events in the dendritic tree may be actually an order of magnitude shorter (Softky, 1994). While the direct experimental evidence in support of this scenario will presumably require *in vivo* recordings, it is reasonable to conclude that, in comparison to pyramidal neurones, the above described classes of interneurones are predisposed to act as coincidence detectors.

As reasoned above, relatively few, in the range of ten presynaptic, temporally correlated inputs may be necessary to trigger a suprathreshold response, assuming resting membrane potentials similar to those obtained under *in vitro* conditions. This particular network property may also explain why excitatory feedback synapses arising from a multitude of presynaptic converging pyramids may be distributed over the entire somato-dendritic surface of some interneurones. If the recurrent input was concentrated on a particular membrane compartment, it may increase the degree of local shunting and thus reduce the efficacy of response summation (Bernander, Douglas, Martin & Koch, 1991).

Activity-dependent modulation of recurrent pyramidal cell input to interneurones

When activating postsynaptic interneurones with pairs of pyramidal cell action potentials, three of the interactions showed a relatively small, albeit statistically significant degree of paired-pulse depression. These results appear to be at variance with findings obtained in slices of rat somatomotor cortex, where pyramid-to-interneurone connections exhibit paired-pulse facilitation (Thomson *et al.* 1993*b*, 1995), whereas in pyramid-to-pyramid interactions paired-pulse depression appears to predominate (Thomson *et al.* 1993*a*). Apart from the obvious differences with regard to species, brain area and age, two further reasons may account for this seeming discrepancy of experimental findings on pyramid-to-interneurone connections. First, pyramid-to-interneurone connections in the rat somatomotor cortex recorded *in vitro* reveal many apparent failures of transmission, thus presumably operating with a relatively low probability of release (Thomson *et al.* 1993*b*). In contrast, the statistical analysis of pyramid-to-interneurone pairs in the cat visual cortex indicates that our experimental conditions appear to favour distinctly higher release probabilities, i.e. conditions which would generally favour the predominance of paired-pulse depression (Zucker, 1989). Second, the frequency and interval of trial episodes are additional factors which may affect the degree of paired-pulse modulation. Increases in the frequency of presynaptic spike trains can also result in a gradual reduction of the degree of paired-pulse facilitation at pyramid-to-interneurone connections (Thomson *et al.* 1995).

Apart from an overall small degree of paired-pulse depression, further analysis indicated that those EPSPs which followed a conditioning first event were relatively little affected by either the amplitude of the preceding event or the inter-event interval. With respect to the lack of or relatively weak correlation of first and second EPSP amplitudes similar observations were also reported in the rat somatomotor cortex (Thomson *et al.* 1995). It thus appears that, within the constraints of our experimental procedures and the interneurone types examined, transmission at cat cortical pyramid-to-interneurone connections is relatively little affected by preceding activity. It follows therefore that, regardless of presynaptic firing rate and/or pattern, presynaptic suprathreshold activity is faithfully transformed into postsynaptic responses. Due to the relatively large stochastic fluctuations in amplitude of both first and second EPSPs this conclusion is perhaps of relatively little functional consequence for unitary, i.e. individual, connections. However, with regard to cortical population activity, it is reasonable to assume that this extrapolation remains valid, since the fairly high probability of finding pyramid-to-interneurone connections in slice preparations (see also Thomson *et al.* 1995) indicates that some types of cortical local-circuit neurones receive large-scale converging input from neighbouring principal neurones. Therefore, the summed input of many presynaptic cells may not be appreciably affected by the stochastic variability of individual interactions.

Amplitude fluctuations of unitary EPSPs in pyramidal cell-to-interneurone connections

The amplitude distributions could be adequately fitted by a sum of double Gaussian functions with variances equal to the noise variances (fully unconstrained model). The fully unconstrained model was not significantly better than a model with the same number of components separated by a constant increment (quantal model). Under the quantal model for transmitter release, these results, in the absence of information regarding the number of electron microscopically determined synaptic junctions, could be interpreted as consistent with the idea that each bouton behaves in an all-or-nothing manner, with minimal quantal variance (Jack, Redman & Wong, 1981). However, the electron microscopic information leads to questions about this interpretation. We found that, in addition to the failure peak, the number of components necessary to fit the experimental amplitude distribution exceeded the number of electron microscopically determined synaptic junctions. This result suggests that a simple quantal model without quantal variance cannot account for the experimental data obtained in these connections. Under the quantal hypothesis, two alternative models emerge: either quantal variance may be present, or some of the release sites might release more than one quantum.

Quantal amplitude. Estimates of quantal amplitudes ranged between 222 and 557 μV for the model without quantal variance, and between 260 and 656 μV for the quantal model with variance and even larger values were obtained for the compound binomial model. These estimates are at the upper range of estimates for quantal sizes of central EPSPs recorded with microelectrodes (e.g. Redman, 1990). The proximal placement of the synapses and electrotonic compactness of the interneurones may contribute to these large amplitudes. It is also possible that the quantal size at each junction is genuinely larger on interneurones relative to pyramidal cells, because glutamatergic synapses on hippocampal GABAergic interneurones have a higher density of AMPA-type glutamate receptors than those on pyramidal dendritic spines (Baude, Nusser, Molnár, McIlhinney & Somogyi, 1995). In addition, a different subunit composition of the glutamate receptors on interneurones might also contribute (Koh *et al.* 1995).

Quantal variance. Two sources may give rise to quantal variance: either within a site (type I variance), or between sites (type II variance; Walmsley, 1993). In the present analysis, only within-site variance was considered. By incorporating quantal variance in addition to the noise variance, adequate fits were obtained for all connections, with a number of components which, excluding the failure peak, were either the same as, or smaller than the number of synaptic junctions detected by the electron microscopic examination. The quantal variance estimated for the

minimum number of components in the quantal model with variance was relatively large, with a quantal coefficient of variation ranging between 0·33 and 0·46. However, for the input to the double bouquet cell (1412942; Fig. 6), models with less quantal variance and a higher number of components, which were still consistent with the structural data, fitted equally well. Indeed, the best-fitting model with seven components in addition to the failure peak, had a relatively small coefficient of variation of 0·12. It is notable that proximal excitatory synapses on double bouquet cells show a characteristic ultrastructural feature – synaptic junctions invaginated into the dendrites (Tamás *et al.* 1997). These characteristic synaptic junctions were not detected on the other types of interneurone (Tamás *et al.* 1997). The possibility therefore exists that quantal properties may vary between different classes of synapses.

Notably, the estimated quantal coefficient of variation for the pyramid-to-basket cell connection with only one synaptic junction (0·45) was similar to the estimates obtained at the two other pyramid-to-basket cell connections. These values are also within the range of the estimated quantal variance reported for single synaptic junctions between pyramidal cells and interneurones (including basket cells) in the CA3 area of guinea-pig hippocampus (0·21–0·53; Gulyás *et al.* 1993). Since type II variance, by definition, cannot exist in connections with only one release site, this result suggests that type I variance can account for most of the variance in excess of the noise variance.

By incorporating quantal variance, a binomial model could also adequately account for the experimental data for two of the connections with more than one release site. It, however, failed to fit the data from the two other connections with more than one release site. Such a failure of binomial models to consistently fit the amplitude fluctuations of EPSPs has been reported for other excitatory connections (e.g. Stricker, Field & Redman, 1996).

If quantal variance was not included in the amplitude fluctuation model, more amplitude components were required, excluding the failures, than the number of electron microscopically determined synaptic junctions. This result also held for the connection with only one synaptic contact, excluding the possibility, at least for this junction, that intersite variance of the quantal size could account for the excess of amplitude components. Since we could not statistically reject this model against the quantal model with variance, from these data we cannot exclude the possibility that single boutons may release more than one quantum.

Release probabilities. The apparent failure rate was relatively low for all connections, ranging from 0·02 to 0·12. This result suggests that at these connections transmission occurs with high reliability. For the three connections with one or two synaptic junctions, incidentally those with post-synaptic basket cells, the data also indicate a high probability of release in at least one synaptic junction. Under a uniform binomial model for transmitter release, the estimated junctional release probability for these connections exceeded 0·7. For the connection with structural evidence for seven synaptic junctions (1412942; Fig. 6) the statistical estimate of the minimum number of release sites was only four, and a uniform binomial model for transmitter release from four sites could account for the amplitude distribution. Thus, in this connection, up to three of the seven release sites could be functionally silent. Since the seven synaptic contacts in this connection were clustered in four groups, each group converging on one dendritic segment, it is possible that each *group* of release sites contributed one quantum, the underlying idea being that closely spaced release sites do not operate independently, or, alternatively, that the apparent quantal size might reflect the synaptic activation of a dendritic segment, rather than a quantal release.

Properties of recurrent pyramid-to-interneurone connections: furthering the understanding of recurrent inhibitory microcircuits

In all five interactions the inhibitory axon showed some degree of spatial overlap with the dendritic arbor of the presynaptic pyramids. Moreover, in two instances both cells were reciprocally connected. It thus appears that with regard to the columnar structure of cat visual cortex these circuits provide the substrate for an inhibitory feedback system in which the activity of principal neurones is influenced by GABAergic interneurones with similar receptive field properties. Despite some degree of similarity in axonal and dendritic patterns of all GABAergic neurones which were shown to receive recurrent pyramidal cell input, the cells could be unequivocally attributed to three distinct, non-overlapping categories (Tamás *et al.* 1997). Although it is not yet known whether other GABAergic local-circuit neurones, such as axo-axonic or neurogliaform cells (Somogyi, 1989), receive recurrent pyramidal cell input, it is clear that *at least* three classes of GABAergic neurones, different with respect to their target selectivity, mediate recurrent inhibitory feedback. Extrapolating from the different target profile of these interneurones it thus follows that recurrent inhibition will be channelled to three distinct compartments on the somato-dendritic surface of principal cells.

Regarding the properties of the unitary recurrent pyramid-to-interneurone EPSPs reported here, notably their reliability, amplitude and temporal characteristics, several important implications emerge which bear immediate relevance for the function of these connections. First, all interactions were highly reliable, with a failure rate of less than 15%. Second, the postsynaptic response was invariably relatively small, on average ~1 mV, and thus generally of insufficient strength to generate suprathreshold responses. Third, the EPSPs had a rapid time course, with EPSP half-widths of less than 6 ms. Temporal integration of converging inputs would therefore be limited to a very narrow time window, where effective summation can occur. Fourth, taking frequency depression of the unitary synaptic responses into account, it is reasonable to assume that the activation of an

interneurone critically depends on concomitant, highly synchronous activity in several pyramidal cells. In turn, due to the large number of synaptic contacts which these interneurones establish in a partly column-specific manner (Tamás *et al.* 1997) individual GABAergic interneurones, such as basket cells, can reliably synchronize the activity of principal cells, as demonstrated in the hippocampus (Cobb *et al.* 1995). In network terms, some of the recurrent inhibitory circuit analysed here may therefore support stimulus-specific synchronization, as recorded in the cat visual cortex *in vivo* (Singer & Gray, 1995). Thus, the functional properties of the unitary interactions reported here suggest that the timing of synaptic events is supported by well-differentiated synaptic circuits in the neocortex.

Baude, A., Nusser, Z., Molnár, E., McIlhinney, R. A. J. & Somogyi, P. (1995). High-resolution immunogold localization of AMPA type glutamate receptor subunits at synaptic and non-synaptic sites in rat hippocampus. *Neuroscience* **69**, 1031–1055.

Bernander, O., Douglas, R. J., Martin, K. A. C. & Koch, C. (1991). Synaptic background activity influences spatiotemporal integration in single pyramidal cells. *Proceedings of the National Academy of Sciences of the USA* **88**, 11569–11573.

Buhl, E. H., Halasy, K. & Somogyi, P. (1994). Diverse sources of hippocampal unitary inhibitory postsynaptic potentials and the number of synaptic release sites. *Nature* **368**, 823–828.

Buhl, E. H., Tamás, G. & Somogyi, P. (1995). Recurrent unitary EPSPs evoked in anatomically identified interneurones of the cat visual cortex *in vitro*. *Journal of Physiology* **487.P**, 51*P*.

Buhl, E. H., Tamás, G., Szilágyi, T., Paulsen, O. & Somogyi, P. (1996). Paired-pulse depression of unitary pyramid to interneuron EPSPs in cat visual cortex *in vitro*. *Society for Neuroscience Abstracts* **22**, 198.8.

Cobb, S. R., Buhl, E. H., Halasy, K., Paulsen, O. & Somogyi, P. (1995). Synchronization of neuronal activity in hippocampus by individual GABAergic interneurons. *Nature* **378**, 75–78.

Davison, A. C., Hinkley, D. V. & Schechtman, E. (1986). Efficient bootstrap simulation. *Biometrika* **73**, 555–566.

Deuchars, J. & Thomson, A. M. (1995). Innervation of burst firing spiny interneurons by pyramidal cells in deep layers of rat somatomotor cortex: paired intracellular recordings with biocytin filling. *Neuroscience* **69**, 739–755.

Erwin, E., Obermayer, K. & Schulten, K. (1995). Models of orientation and ocular dominance columns in the visual cortex: a critical comparison. *Neural Computation* **7**, 425–468.

Eysel, U. T., Crook, J. M. & Machemer, H. F. (1989). GABA-induced remote inactivation reveals cross-orientation inhibition in the cat striate cortex. *Experimental Brain Research* **80**, 626–630.

Gilbert, C. D. (1983). Microcircuitry of the visual cortex. *Annual Review of Neuroscience* **6**, 217–247.

Gulyás, A. I., Miles, R., Sík, A., Tóth, K., Tamamaki, N. & Freund, T. F. (1993). Hippocampal pyramidal cells excite inhibitory neurons through a single release site. *Nature* **366**, 683–687.

Han, Z.-S., Buhl, E. H., Lörinczi, Z. & Somogyi, P. (1993). A high degree of spatial selectivity in the axonal and dendritic domains of physiologically identified local-circuit neurons in the dentate gyrus of the rat hippocampus. *European Journal of Neuroscience* **5**, 395–410.

Jack, J. J. B., Redman, S. J. & Wong, K. (1981). The components of synaptic potentials evoked in cat spinal motoneurones by impulses in single group I a afferents. *Journal of Physiology* **321**, 65–96.

Kawaguchi, Y. & Kubota, Y. (1993). Correlation of physiological subgroupings of nonpyramidal cells with parvalbumin- and calbindinD28k-immunoreactive neurons in layer V of rat frontal cortex. *Journal of Neurophysiology* **70**, 387–396.

Kisvarday, Z. F., Martin, K. A. C., Freund, T. F., Magloczky, Z., Whitteridge, D. & Somogyi, P. (1986). Synaptic targets of HRP-filled layer III pyramidal cells in the cat striate cortex. *Experimental Brain Research* **64**, 541–552.

Kisvarday, Z. F., Martin, K. A. C., Whitteridge, D. & Somogyi, P. (1985). Synaptic connections of intracellularly filled clutch cells: a type of small basket cell in the visual cortex of the cat. *Journal of Comparative Neurology* **241**, 111–137.

Koh, D.-S., Geiger, J. R. P., Jonas, P. & Sakmann, B. (1995). Ca^{2+}-permeable AMPA and NMDA receptor channels in basket cells of rat hippocampal dentate gyrus. *Journal of Physiology* **485**, 383–402.

König, P., Engel, A. K. & Singer, W. (1996). Integrator or coincidence detector? The role of the cortical neuron revisited. *Trends in Neurosciences* **19**, 130–137.

Maccaferri, G. & McBain, C. J. (1995). Passive propagation of LTD to stratum oriens-alveus inhibitory neurons modulates the temporoammonic input to the hippocampal CA1 region. *Neuron* **15**, 137–145.

Mason, A., Nicoll, A. & Stratford, K. (1991). Synaptic transmission between individual pyramidal neurons of the rat visual cortex *in vitro*. *Journal of Neuroscience* **11**, 72–84.

Paulsen, O., Stricker, C., Tamás, G., Szilágyi, T., Somogyi, P. & Buhl, E. H. (1996). Quantal variance revealed in electron microscopically identified excitatory synapses of the cat visual cortex. *Society for Neuroscience Abstracts* **22**, 206.3.

Redman, S. (1990). Quantal analysis of synaptic potentials in neurons of the central nervous system. *Physiological Reviews* **70**, 165–198.

Sillito, A. M. (1992). GABA mediated inhibitory processes in the function of the geniculo-striate system. *Progress in Brain Research* **90**, 349–384.

Singer, W. & Gray, C. M. (1995). Visual feature integration and the temporal correlation hypothesis. *Annual Review of Neuroscience* **18**, 555–586.

Softky, W. (1994). Sub-millisecond coincidence detection in active dendritic trees. *Neuroscience* **58**, 13–41.

Somogyi, P. (1989). Synaptic organisation of GABAergic neurons and $GABA_A$ receptors in the lateral geniculate nucleus and visual cortex. In *Neural Mechanisms of Visual Perception. Proceedings of the Retina Research Foundation Symposia*, ed. Lam, D. K.-T., Gilbert, C. D., pp. 35–62. Portfolio Publications, The Woodlands, TX, USA.

Spruston, N., Jaffe, D. B. & Johnston, D. (1994). Dendritic attenuation of synaptic potentials and currents: the role of passive membrane properties. *Trends in Neurosciences* **17**, 161–166.

Stern, P., Edwards, F. A. & Sakmann, B. (1992). Fast and slow components of unitary EPSCs on stellate cells elicited by focal stimulation in slices of rat visual cortex. *Journal of Physiology* **449**, 247–278.

Stricker, C., Field, A. C. & Redman, S. (1996). Statistical analysis of amplitude fluctuations in EPSCs evoked in rat CA1 pyramidal neurones *in vitro*. *Journal of Physiology* **490**, 419–441.

Stricker, C., Redman, S. & Daley, D. (1994). Statistical analysis of synaptic transmission: model discrimination and confidence limits. *Biophysical Journal* **67**, 532–547.

TAMÁS, G., BUHL, E. H. & SOMOGYI, P. (1997). Fast IPSPs elicited via multiple synaptic release sites by different types of GABAergic neurone in the cat visual cortex. *Journal of Physiology* **500**, 715–738.

THOMSON, A. M., DEUCHARS, J. & WEST, D. C. (1993*a*). Large, deep layer pyramid–pyramid single axon EPSPs in slices of rat motor cortex display paired-pulse and frequency dependent depression, mediated presynaptically and self-facilitation, mediated postsynaptically. *Journal of Neurophysiology* **70**, 2354–2369.

THOMSON, A. M., DEUCHARS, J. & WEST, D. C. (1993*b*). Single axon excitatory postsynaptic potentials in neocortical interneurons exhibit pronounced paired pulse facilitation. *Neuroscience* **54**, 347–360.

THOMSON, A. M., WEST, D. C. & DEUCHARS, J. (1995). Properties of single axon excitatory postsynaptic potentials elicited in spiny interneurons by action potentials in pyramidal neurons in slices of rat neocortex. *Neuroscience* **69**, 727–738.

THURBON, D., FIELD, A. & REDMAN, S. (1994). Electrotonic profiles of interneurons in stratum pyramidale of the CA1 region of rat hippocampus. *Journal of Neurophysiology* **71**, 1948–1958.

WALMSLEY, B. (1993). Quantal analysis of synaptic transmission. In *Electrophysiology: A Practical Approach*, ed. WALLIS, D. I., pp. 109–141. IRL Press, Oxford.

WILKS, S. S. (1938). The large-sample distribution of the likelihood ratio for testing composite hypotheses. *Annals of Mathematical Statistics* **9**, 60–62.

YUSTE, R. & TANK, D. W. (1996). Dendritic integration in mammalian neurons, a century after Cajal. *Neuron* **16**, 701–716.

ZUCKER, R. S. (1989). Short-term synaptic plasticity. *Annual Review of Neuroscience* **12**, 13–31.

Acknowledgements

We are grateful to Mr J. D. B. Roberts for technical assistance and to Mr P. Jays and Mr F. Kennedy for their photographic support. We gratefully acknowledge the use of a DEC Alphastation at the MRC Facility for Computational Modelling in Cognitive Science, Department of Experimental Psychology, Oxford. O.P. is the Christopher Welch Junior Research Fellow at Wadham College, Oxford. During part of this project G.T. was recipient of the Oxford–Szeged Scholarship and the Blaschko Visiting Research Scholarship of Oxford University.

Author's email address

E. H. Buhl: eberhard.buhl@pharm.ox.ac.uk

Received 29 July 1996; accepted 24 January 1997.